Applied Energy 388 (2025) 125643

Contents lists available at ScienceDirect

Applied Energy

journal homepage: www.elsevier.com/locate/apen

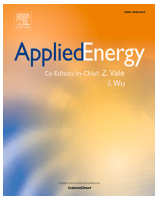

A hybrid Gaussian process-integrated deep learning model for retrofitted building energy optimization in smart city ecosystems

Behnam Mohseni-Gharyehsafa [a,*], Shahid Hussain [b,c,**], Amy Fahy [d,f], Mattia De Rosa [e], Fabiano Pallonetto [d,f]

[a] Centre for Ocean Energy Research, Maynooth University, Maynooth, Co. Kildare, Ireland
[b] Innovation Value Institute (IVI), School of Business, National University of Ireland Maynooth (NUIM), Maynooth, W23 F2H6, Co. Kildare, Ireland
[c] Department of Computing, South East Technological University (SETU), Carlow Campus, Carlow, R93 AYW9, Ireland
[d] International Renewables and Energy Systems Integration (IRESI), School of Business, National University of Ireland Maynooth, Maynooth Co. Kildare, Ireland
[e] Dipartimento di Ingegneria Meccanica ed Energetica, Università di Genova, Genova Italy
[f] School of Business, Maynooth University, Maynooth, Co., Kildare, Ireland

HIGHLIGHTS

- Formulated energy intensity metrics and primary factors to optimize retrofitting efficiency.
- Integrated Gaussian Process (GP) model with Deep Learning for smarter energy optimization.
- Designed an architecture highlighting functional components of the GP-Deep learning framework.
- Investigated energy dynamics of 6076 buildings in Mullingar City, Ireland, urban and suburban.

ARTICLE INFO

Keywords:
Energy community
End-user intensity
Hybrid Gaussian process-DL
Primary energy factor
Retrofitted buildings
Smart city

ABSTRACT

Traditional retrofitting methods need a considerable upgrade; therefore, they often require significant time and financial investment, and can disrupt the building operations and occupant activities during implementation. Consequently, developing fast-response retrofitting solutions to save energy on urban and large scales is critical for city planners and policymakers. This study integrates a Gaussian Process-based Deep Learning (GPDL) model to retrofit buildings on a metropolitan scale, aiming to accelerate the transition towards smart cities. Gaussian Process offers a probabilistic approach to assess uncertainty in data points, while deep learning captures complex data patterns. The hybrid approach enhances the accuracy and reliability of end use intensity (EUI) predictions, ultimately supporting the computation of the primary energy factor (PEF) for improved decision-making in energy management. The proposed GPDL model was applied to a case study consisting of 6076 buildings in Mullingar City, which is located in Westmeath County, Ireland. The case study evaluated various heating, ventilation, and air conditioning systems (HVAC) such as gas boilers, electric heaters, and heat pumps, as well as different wall structures with distinct insulation layers in retrofitted buildings. The results demonstrated a reduction of EUI by about 52.4 %, resulting in 39.2 % energy savings for the overall city, with the proposed GPDL. The developed GPDL presented high accuracy mean square error: 1.3005, root-mean-square error: 0.0036, and mean absolute percentage error: 0.0022, leading to rapid EUI predictions within seconds, compared to the state-of-the-art linear and spline regression models, which require hours for similar estimations. The findings also underscored that the choice of heating, water system, HVAC, fans, interior lighting, electric equipment, pump, and gas equipment system has a greater impact on EUI than wall structure, leading to valuable recommendations of natural gas or renewable energy sources due to lower primary energy factor for urban planners focused on developing smart cities.

* Corresponding author.
** Corresponding author at: Innovation Value Institute (IVI), School of Business, National University of Ireland Maynooth (NUIM), Maynooth, W23 F2H6, Co. Kildare, Ireland
Email addresses: behnam.mohsenigharyehsafa.2023@mumail.ie (B. Mohseni-Gharyehsafa), shahid.hussain@mu.ie (S. Hussain), amy.fahy@mu.ie (A. Fahy), mattia.derosa@unige.it (M. De Rosa), fabiano.pallonetto@mu.ie (F. Pallonetto).

https://doi.org/10.1016/j.apenergy.2025.125643
Received 13 December 2024; Received in revised form 22 January 2025; Accepted 25 February 2025
Available online 19 March 2025

Symbols

$\delta(x - x')$	Kronecker Delta Function
σ^2	Noise Variance
$\mu(x)$	Mean Function at x
Σ	Variance–covariance Matrix
Φ	Function-space Mapping
θ	Hyperparameters of the Model
$\mathbb{E}$	Expectation Operator (mean)
$\overline{f(x)}$	Mean function at x
$\mathbb{V}$	Variance operator
$\mathcal{GP}$	Gaussian Process
$\mathcal{N}$	Normal distribution
$\mathcal{K}$	Kernel function
C	Constant value in kernel function
l	Length scale parameter in RBF kernel
I	Spread/Projection of Kernel Function
X	Input feature vector
Y	Output target vector
Cov	Covariance
D	Domain
RBF	Radial Basis Function
$\mathcal{F}$	Concatenation Function
f_θ	DL Model
$\hat{\sigma}_{GP}$	Estimated Uncertainty of GP Model

Variables

A_B	Total floor area of building B [m^2]
A_{Total}	Total floor area of all buildings
E_B	Total energy consumption of building B [kWh]
$E_{i,t}$	Energy consumption of device i at time t [kWh]
EUI	End Use Intensity [$kWh \cdot m^{-2}$]
$\widehat{EUI}$	Predicted EUI from GPDL model [$kWh \cdot m^{-2}$]
PEF	Primary Energy Factor [−]
Std	Standard deviation
$SPES$	Specific Primary Energy Source [$kWh \cdot m^{-2}$]
T	Maximum Time
t	Time Step
$Temp$	Temporary variables

Abbreviations

ANN	Artificial Neural Network
AIC	Akaike Information Criterion
API	Application Programming Interface
AHP	Analytic Hierarchy Process
BIC	Bayesian Information Criterion
CBR	Case-Based Reasoning
CK	Constant Kernel
CDF	Cumulative Distribution Function
DHW	Domestic Hot Water Standard Deviation
FNN	Feedforward Neural Network
G	Gas Energy Source
GP	Gaussian Process
$GPDL$	Gaussian Process-based Deep Learning
GPS	Global Positioning System
HP	Heat Pump
DL	Deep Learning
$RMSE$	Root Mean Squared Error
RES	Renewable Energy Source
MBE	Mean Bias Error
MSE	Mean Squared Error
MAE	Mean Absolute Error
$MAPE$	Mean Absolute Percentage Error
$PINAW$	Prediction Interval Normalized Average Width
$NLPD$	Negative Log Predictive Density
RBF	Radial Basis Function
GHG	Greenhouse Gas
$HVAC$	Heating, Ventilation, and Air Conditioning
$I.S.$	Irish Standard
$CAPEX$	Capital Expenditures
AI	Artificial Intelligence
GA	Genetic Algorithm
RF	Random Forest
kWh	kilowatt Hour
$NSAI$	National Standards Authority of Ireland
PV	Photovoltaic
$Q-Q$	Quantile–Quantile
OSM	Open Street Map tool
O	Other Energy Sources (i.e., peat, biomass, RESs)
W	White Kernel

1. Introduction

1.1. Background study

Buildings account for approximately 30–40 % of global energy consumption, making the building sector one of the largest energy consumers worldwide, and thus contributing to greenhouse gas (GHG) emissions [1]. The primary sources of energy consumption in buildings are heating, cooling, ventilation, lighting, and powering electronic appliance systems [2]. The energy consumption of these systems is influenced by the building type, age, climatic conditions, and occupancy patterns [2]. Historically, building designs were mainly concentrated on cost-effectiveness and functionality, often compromising on sustainability and energy efficiency, thereby leading to the traditional buildings characterized by high energy consumption [3]. Consequently, in the energy landscape buildings represent an important sector when it comes to global efforts to optimize energy consumption for reducing GHG emissions and mitigating climate change [4].

Retrofitting emerges as an impactful solution for enhancing the energy efficiency of the traditional buildings [1]. Retrofitting measures correspond to updating an outdated and inefficient building's infrastructure, such as heating, ventilation, and air conditioning (HVAC), envelope, insulation, and fenestration, with a more efficient system [5]. The retrofitting scenarios are cost-effective solutions that reduce the energy cost and carbon footprint by utilizing renewable energy vectors such as solar energy, and having efficient HVAC systems, thus contributing to environmental sustainability. Given the material [6], labor, structure modification [7], and utility connection [8] costs, retrofitting existing buildings often comes with significantly higher installation and upgrade costs, leading to an increase in capital expenditures (CAPEX) [9]. Retrofitting the existing buildings requires the consideration of several key factors including: the energy system, building envelope, the energy vector, and building occupancy [10]. The energy system is characterized by the HVAC system [11], the building envelope consists of the heat conductance and the air leakage [12], the energy vector holds the energy generation sources such as fossil fuel, renewable (e.g., solar, wind, and heat pump) [13] and the energy carrier systems (e.g., high, medium, and low voltage systems along with substations), while the building occupancy deals with the people in the buildings and their comfort level. Consequently, retrofitting existing buildings represents a complex process and thereby requires sophisticated solutions that are not only cost-effective but also support desired building efficient operations [14].

1.2. Importance of AI in retrofitting buildings

It is evident that adopting an effective retrofit measure is a complex and challenging task that requires evaluating adaptive scenarios to determine the most optimum case in relation to each building's environment [13]. Recent advancements in artificial intelligence (AI) technology (e.g., machine learning and deep learning) are emerging as pivotal solutions for optimizing retrofitting scenarios [15] that enable data-driven approaches [16] for decision-making to achieve cost, energy, and environmental efficiency in building operations [17]. In more detail, a well-trained AI system has the capability to comprehend the building energy consumption pattern and detect the mainstreams of energy leaks. It can also expand the findings by suggesting suitable retrofitting scenarios based on spatio-temporal requirements to the local decision makers, aiming to minimize energy waste in the energy community [18]. These AI-enabled systems support advanced knowledge of energy consumption and offer intelligent solutions to schedule the building energy system based on their corresponding occupancy behavior, ventilation and heating time, and hot water usage. However, the AI-enabled models for retrofitting building scenarios are data-hungry [19], longer training time [20], utilization of higher computational resources, suffering from poor parameter tuning [21], comprehending the end-user intensity, and primary energy factors (PEFs), leading to underfitting and overfitting [22] issues. Given the interdisciplinary energy consumption in a diverse building community where numerous factors such as building envelope materials, HVAC systems [23], occupancy schedules, dynamic tariffs [24], etc. are involved, such limitations often mislead the optimum decision-making in large-scale smart city scenarios.

1.3. Knowledge gap and our contribution

While AI-enabled models are considered powerful tools with potential for solving complex retrofitting problems, they pose several open challenges when applied to building retrofitting. These challenges include their dependency on large datasets [19], high computational costs [20], issues related to model parameterization [21], inability to capture critical factors effectively [25], and performance limitations [22]. Furthermore, the interdisciplinary nature [26] of energy consumption in retrofitted buildings, dynamic usage patterns driven by stochastic occupant behavior, and fluctuating energy costs [24] create highly complex retrofitting scenarios. These complexities [26] and the open challenges associated with the AI-enabled models [21] portray an evident knowledge gap and necessitate the development of robust models capable of accurately capturing comprehensive energy consumption patterns while delivering efficient performance. To bridge this knowledge gap, this work introduces a hybrid approach that integrates the Gaussian Process (GP) with Deep Learning (DL), aiming to: accelerate the transition of retrofit buildings towards smart cities. In the developed GPDL model, the GP efficiently captures the uncertainties inherited in the data points, while the DL learning captures complex data patterns to enhance the accuracy and reliability of end use intensity (EUI) predictions. This ultimately supports the computation of the PEF for improved decision-making in energy management. The contributions of this investigation are:

- Developed a hybrid data-driven approach based on the integration of Gaussian-Process with deep learning aiming to enhance the prediction of the EUI, reduce the computational complexity, and recommend the primary energy source for the heating, water system, HVAC, fans, interior lighting, electric equipment, pump, and gas equipment system.
- Established a detailed architecture highlighting the functional components of retrofitting buildings in conjunction with the developed GPDL. Moreover, a detailed formulation for the EUI and PEF is established and a detailed mathematical modeling for integrating the Gaussian Process with deep learning is presented. In addition, a detailed characterization and exploration of the various retrofitted buildings is presented and mathematically coupled with the developed GPDL model.
- Conducted a detailed case study on the retrofitted buildings in Mullingar city and tested the case study on the developed GPDL model. A comprehensive evaluation criterion is established from the EUI, PEF, deep retrofitted analysis, and model performance. Given the evaluation criteria, the performance of the proposed GPDL is evaluated against state-of-the-art linear [27] and spline [28] regression models. The results demonstrate a reduction of EUI by about 52.4 %, resulting in 39.2 % energy savings for the overall city with high accuracy (MSE: 1.3005, RMSE: 0.0036, and MAPE: 0.0022). This leads to rapid EUI predictions within seconds, compared to the state-of-the-art linear and spline regression models, which require hours for similar estimations.

1.4. Paper organization

The structure of the study is as follows: in Section 2, an up-to-date review of the literature is provided. The methodology followed by the case study is described in Section 3. The simulation setup, performance evaluation criteria, and results with discussions are formulated in Section 4. The implications of the investigation and the ways to accelerate the pace towards a smart city as a useful guide for urban designers are articulated in Section 4.7. Finally, the paper is concluded with possible future direction in Section 5.

2. Literature review

Retrofitting the existing building has a paramount impact on energy efficiency, carbon emission reduction, and addressing end-user's thermal comfort and expenses. The multidimensional aspect of buildings in cities and communities, ranging from heterogeneous combinations of size, and architecture to diverse HVAC systems, makes retrofitting a formidable task [26]. Artificial intelligence, as an emerging transformative solution, empowers decision makers and urban planners to have reliable and accurate models with much less laborious effort in the minimum required time [18]. Consequently, the applications of AI in retrofitting have captured the interest of researchers, and in the literature, AI-enabled retrofitting has been studied from the perspectives of energy communities and smart cities, as presented in the following.

Zhao et al. [29] gathered 71 retrofitted buildings in China. They used distinct features of retrofitting as 1) background information including the age, the size, and type of the building, proprietorship, and the meteorological details, 2) facility information: the insulation situation, and HVAC, lighting, and piping conditions, 3) and energy and cost portfolio such as yearly expenditure, and the available budget and the payback period. They applied the designed case-based reasoning (CBR) approach in a real scenario in Shanghai. They found potential matches for fluorescent LED tubes, automated light systems, glazing, chiller HVAC, insulation of the roof, HVAC control systems, and valves.

In [30], 429 investigations are reviewed regarding case-based applications in building retrofit with a multi-criteria decision-making model. The most commonly used methods were categorized into 4 categories: AI models, questionnaires, simulation software, and statistical hybrid algorithms. In general CBR models follow this 5 step cycle: represent, retrieve, reuse, revise, and retain. The CBR model is not being used widely in architecture, and what is lacking is the retrieval of optimal cases. Two types of weight calculation for CBR cycle classification were recognized: weight factor and non-weight factor computation, and methods like genetic algorithm (GA), analytic hierarchy process (AHP), and artificial neural network (ANN) are commonly used for weight coefficient determination, with AHP being the simplest to integrate. The last finding regards the accuracy of reference cases in CBR depending on user input quality and covers both subjective preferences and objective

architectural information, with changing order significantly impacting outcomes.

Recently, Liu et al. [31] combined random forest (RF) with case-based reasoning to obtain a consolidated decision-making approach to retrofit buildings. The RF is added to the case-based reasoning to support the revision and retaining step. Their methodology can search through 109 sustainability retrofitted projects. Applying the method to a real case study shows a 37 % reduction in the end-use intensity and 19,400 kWh of electricity savings. In another investigation, Johari et al. [18] performed a retrofitting scenario using calibrated urban building energy modeling. The case studies are focused on Swedish households. They study the influence of retrofitting on power flow and power demand. They conclude that energy retrofitting leads to a 7 % voltage increase in the considered case studies at maximum.

Choi et al. [32] used hierarchical clustering to rate the energy performance of retrofitted buildings. They simplified the energy performance of buildings using energy signatures, and the sensitivity of cooling and heating regarding the outdoor conditions. Generally, they classified the retrofitted scenarios into six groups. The developed method is applied to the buildings in South Korea. The analysis shows about 73 % energy signature improvement after retrofitting. Their method can be useful in evaluating the gross benefits of urban size and large-scale retrofitting plans.

In [33], a retrofitting strategy is developed to enhance the energy efficiency of a private city district in Cairo. They considered five case studies where the youngest building was constructed in 2015 and the oldest in 2012. The retrofitting measures are applied to walls, apertures, ceilings, shading, and lighting. The results show an 88.68 % enhancement in energy efficiency in the gated community. Their study shows significant improvement in energy efficiency in private residential sectors. However, the study needs improvement to automate the retrofitting measures in residential private enclaves on a large scale. Note that, high-income family residences in a gated community where applying retrofit can lead to weighty results [34].

Evaluating the energy efficiency of buildings using physics-based models on a large scale is a demanding task that requires time for computation and effort. Artificial intelligence can help the process by reducing the dimension of computation to have a rapid evaluation of the energy portfolio for the decision-making process. Zhang et al. [35] combined three methods to automate the retrofitting measures for houses in Canada: Multi-layer perceptron neural network to identify the system, GA for optimization, and multi-criteria decision-making approach are mixed. The measures applied for retrofitting are regulating the air leakages, wall insulation, and installing heat pumps.

Having a fast engine to evaluate the energy performance of buildings is crucial for retrofitting scenarios consisting of large options. Seyedzadeh et al. [22] present a methodology to evaluate building energy performance rapidly. The method has a valuable feature selection algorithm to identify the influential factors in the building energy and carbon emission portfolio in non-residential buildings in the UK; 43 features have been selected. Three different techniques to develop building energy performance in urban size were established [36]. The methods are ensemble machine learning, parametric simulation, and segregation. Nineteen parameters were used in the model. A large amount of synthetic datasets about 1 million cases are built. The methodology is limited by using categorical building types: terraced, detached, semi-detached, and bungalow in Ireland with default static floor area. The research is focused on annual energy consumption and did not consider different schedules such as monthly and seasonal variations.

In [37], a surrogate model is developed to reduce the computation cost of evaluating energy performance and suggesting retrofit options for residential buildings in Zurich. The proposed surrogate model is a combination of two machine learning techniques with the inputs of type, age, floor area, energy carrier, height, and roof slope and orientation of the building. The computation rate of the simulation is enhanced from minutes to microseconds. The methodology presents a useful tool for large-scale decision-making in retrofit projects. Al-Habaibeh et al. [38] combined infrared thermography images with neural networks to provide a method to evaluate retrofitting scenarios using insulation and combining with solar photovoltaic (PV) panels. The case study is located in Nottingham, UK. The neural network shows promising results with 82 % accuracy.

In [25], machine learning is exploited to gather useful information for Retrofitting possibilities in the UK, by district socio-economic data analysis. In this study, they implemented a method of eXtreme Gradient Boosting to extract building retrofits from the UK EPC data, which can analyze changes in buildings over time. Then the study explores what aspects influenced the retrofit being carried out or not by applying SHapely Additive exPlanations values as an explainable AI technique for the previous method. Sharma et al. [39] present different retrofit strategies that are evaluated with a calibrated simulation approach. The monitored building is a school in Malaysia and the study focuses heavily on the validation of the simulation model created.

Three levels of retrofit are then evaluated for envelope upgrade and compared with the base case aiming to maximize energy consumption reduction. The deepest level of retrofit shows the highest impact in reducing emissions related to air conditioning. The researchers assumed a 25–30-year project to reflect the life-cycle length of retrofit steps, demonstrating a positive Net Present Value and payback period of around 10 years, with a reduction of emissions of around 20 %. In another study, Ma et al. [40] applied four machine learning methods with a case based on 301 retrofitted buildings. They divided the retrofitting measures into 2 categories including building envelope and HVAC systems. XGBoost is the most accurate modeling with a precision of 76 % and 77 % for HVAC retrofitting and envelope retrofitting, respectively.

Most of the studied work focuses on the way to simulate the retrofitting without paying attention to the applicability of the locality or having a model that fully represents the city with the main ingredients and related operations. Note that by aggregating a simple simulated building, having a consolidated presentation of a city is challenging. Buildings' physics have effects on each other and shading is an important issue in energy simulation. Physics-based modeling known as white-box simulations is laborious demanding enough computational capability.

To the best of the author's knowledge, studies developing machine learning models using GP to accurately estimate the end-use intensity of an entire city are extremely rare. The model curbs the challenge of computation and reveals the EUI of the buildings in different retrofitting scenarios in seconds, while the same task using a white-box model requires at least more than 15 hours of simulations with utmost processing unit usage. This model is useful for urban planners and policymakers to have a reliable rapid estimation of the EUI of a city not only for retrofitting but also for creating new cities and enhancing urbanization and smart cities.

3. Proposed Gaussian process-based deep learning model for retrofitting buildings

This work develops a GPDL model to enhance the prediction of EUI for optimal decision-making and improved energy efficiency in retrofitted buildings, as illustrated in Fig. 1. The system model is composed of three main sections. The first section offers an overview of the entire process, giving a broad understanding of the model's functionality. The second section, the blueprint, provides an in-depth representation, detailing the intricacies and structure of the model. The final section, the output, presents the results associated with each subsection of the blueprint, highlighting the outcomes and their implications. The following sections outline the comprehensive methodology of the proposed data-driven approach for retrofitting buildings. This provides a holistic perspective for smart city planners, aimed at significantly enhancing energy efficiency in large-scale retrofitting projects.

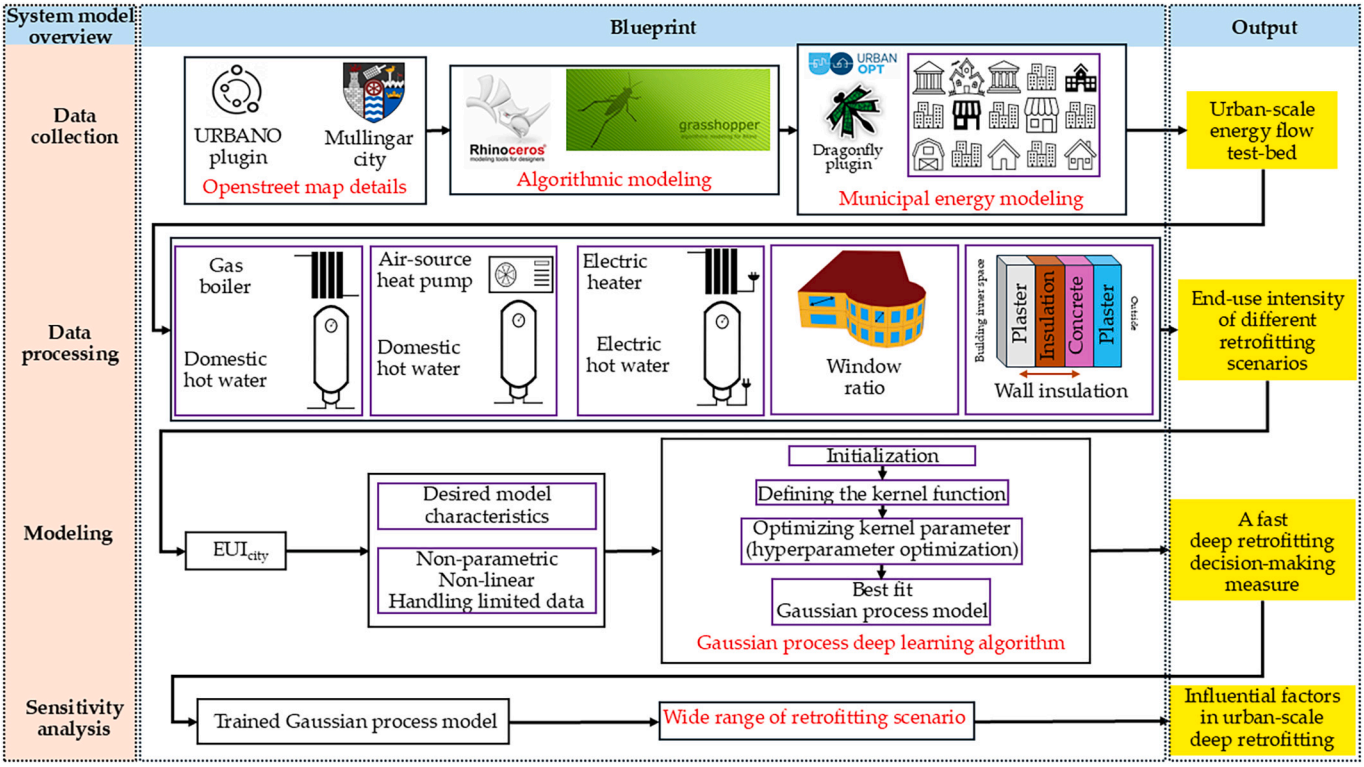

Fig. 1. System model of the proposed Gaussian Process based Deep Learning (GPDL) approach, highlighting the main functional components.

3.1. Problem statement and formulation

Traditional retrofitting methods enhance building performance by upgrading insulation, windows, and HVAC systems, and improving lighting and water heating to reduce energy consumption. However, traditional energy efficiency methods often come with high upfront costs, lack customization for specific building needs, and do not provide real-time monitoring to continuously optimize performance [41]. While deep learning algorithms offer a more cost-effective solution [15], retrofitting on a large city scale significantly increases computational complexity, thereby reducing response times and impacting model accuracy.

To enhance the performance of DL in retrofitting buildings, this work introduces the concept of coupling GP with DL. In the proposed GPDL model, the GP estimates uncertainty and identifies the most informative data points [42], thereby reducing training time. Meanwhile, the DL model captures high-dimensional inputs and extracts features from larger datasets, accelerating convergence and improving model accuracy. In the proposed GPDL model, the target variable is EUI, which is defined as the total energy consumption (E_B) of a retrofitted building divided by its total floor area (A_B), as given in Eq. (1). The EUI serves as a standardized measure for city planners to assess and compare the energy performance of buildings.

$$EUI_{B_1} = \frac{E_{B_1}}{A_{B_1}} \tag{1}$$

where EUI_{B_1} represents the EUI of building (B_1), E_{B_1} is the total energy, and A_{B_1} is the total floor area consumption of a building (B_1). The total floor area of building (B_1) is sum of the floors of each stories in the building. The total energy consumption E_B is a function of the energy usage from various sources and can be calculated according to Eq. (2).

$$E_{B_1} = \sum_{i=1}^{n} \sum_{t=1}^{T} E_{i,t} \tag{2}$$

where $t = \{t_1, t_2, \cdots, T\}$ is the time domain, n is the total number of energy devices, i is the index of the energy consumption devices such that $i = \{E_{gas\ boiler}, E_{heat\ pump}, \cdots, E_n\}$. The EUI of all the buildings in the city can be thus computed by aggregating the individual building energy consumption in the city as presented in Eq. (3).

$$\begin{cases} EUI_{city} = \dfrac{1}{A_{total}} \displaystyle\sum_{j=1}^{N} EUI_j \times A_j \\ A_{total} = \displaystyle\sum_{j=1}^{N} A_j \end{cases} \tag{3}$$

where N is the total number of buildings in the city. A_{total} is the sum of all buildings floor area.

Following the formulation of the target variable the inputs $E = \{E_{B_1}, E_{B_2}, \cdots, E_{B_N}\}$ and $A = \{A_{B_1}, A_{B_2}, \cdots, A_{B_N}\}$, are determined based on Eqs. (1) and (2) and is linked to the input space (X) through the function ($\mathcal{F}$), as given in Eq. (4).

$$X = \mathcal{F}(E, A) \tag{4}$$

where $\mathcal{F}$ is a concatenation function for defining the input space. Once the input space and the target variable are formulated the GP and the DL functions can be defined based on the input and target variables as given in Eqs. (5) and (6).

$$\hat{\sigma}_{GP}(x_*) = \mathcal{GP}(X) \tag{5}$$

$$\widehat{EUI}_{DL} = f_\theta(X) \tag{6}$$

where f_θ represents the DL model with parameters θ represents the GP model, $\hat{\sigma}_{GP}$ is the estimated uncertainty of the GP model for the new variable (x_*) and $\widehat{EUI}_{DL}$ is the predicted output of the DL model. To enhance prediction performance, we introduce a novel hybrid modeling

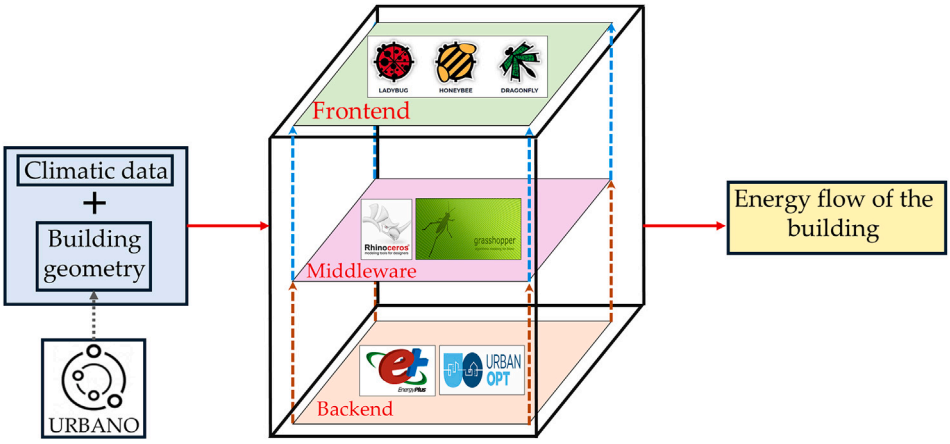

Fig. 2. Energy simulation framework integrating backend, middleware, and frontend tools for building and urban energy flow analysis.

approach that synergistically integrates a DL model with the estimated uncertainty of a GP model, as detailed in Eq. (7). Kernel function and marginal likelihood concept is used to perform hyperparameter optimization [43].

$$\widehat{EUI} = GPDL\left(f_\theta(X), \hat{\sigma}_{GP}(x_*)\right) \tag{7}$$

Once the problem has been defined, the subsequent sections delve into the modeling of municipal energy buildings, a detailed procedure for deriving the GP using Gaussian distribution techniques, as well as the development and implementation of a deep learning model. Moreover, the pseudocodes (Algorithm 1 and Algorithm 2) for the development of the proposed model are also presented.

3.2. Modeling of the municipal energy buildings

To develop a 3D model of municipal energy buildings, this study employs a range of tools and methodologies. Specifically, it leverages OpenStreetMap (OSM)[1] for geographic data, integrates master planning techniques to guide spatial organization, utilizes Grasshopper for parametric design, and conducts environmental analysis using Dragonfly plugins [44]. This approach ensures a comprehensive and detailed representation of energy buildings at the municipal level, incorporating both spatial and environmental considerations.

3.2.1. Construction of geographic building

To establish a 3D construct of the building, we utilize URBANO,[2] an OSM tool, that creates a free, and editable map of the world. The OSM platform enables the users to post and manage geographic data, such as roads, trails, cafés, and railway stations. The posting of data can be performed through global positioning system (GPS) devices, aerial images, and other free information sources, where the data are compiled in a centralized accessible database. Consequently, the platform provides freely accessible information for a wide range of creative applications in mobile navigation, technological city planning, and the environment. The dimensions for residential and amenity buildings are calculated following the various Irish building dimensions [45]. The building consists of houses, detached houses, semi-detached houses, terraced houses, apartments, and bungalows amongst other general dwellings. The facility subsystems under the structural division are considered to be the roof, wall, window, and entrance [36].

These different inputs are passed to the OSM application programming interface (API) for creating a wide range of residential buildings, schools, hospitals, public drinking places, and shopping facilities. The master planning data are fed into Dragonfly plugins[3] to evaluate energy consumption and identify opportunities for energy efficiency improvements, utilizing the Grasshopper[4] to evaluate the aggregated annual EUI. The development of the building structure and the HVAC system is presented in the subsequent sections.

Fig. 2[5] presents the energy flow diagram used in this manuscript. EnergyPlus[6] and URBANopt[7] serve as the core backends for energy simulation. EnergyPlus handles building-level energy flow simulations, leveraging its extensive libraries and modules. URBANopt, built on top of EnergyPlus, extends its capabilities to provide solutions at the urban scale. These tools are integrated via Rhinoceros and Grasshopper plugins, which act as middleware within the LadyBug Tools suite. LadyBug Tools offers a user-friendly, frontend interface for advanced building energy simulation software. For building geometries, URBANO, an open-source API compatible with Grasshopper, is employed to generate urban-scale geometries. Climatic data are freely available from various sources, including EnergyPlus and LadyBug Tools. By combining these software tools and resources, energy flows at both the urban area and community building levels can be effectively analyzed and simulated.

3.2.2. Building envelope structure

The National Standards Authority of Ireland (NSAI) provides a range of standards related to building construction, including wall construction to ensure that building practices comply with safety, durability, and environmental performance requirements [46]. The relevant standards for wall construction in Ireland typically include the Irish Standard (I.S.) 325 code of practice for use of masonry [47], I.S. EN 1996 (Eurocode 6) for design of masonry structures [48], I.S. 440 for concrete construction [49], I.S. 189 for the structural use of concrete [50], I.S. 401 for the timber frame construction [51], and I.S. EN 1365 for fire resistance tests [52].

The I.S. 325 covers the design, materials, and workmanship for constructing masonry walls, load bearing, and non-load bearing walls [47]. The I.S. EN 1996 (Eurocode 6) focuses on the design of the masonry structure and consists of different sub-codes including I.S. EN 1996-1-1 that provides general guidelines for reinforced and unreinforced masonry structures, the I.S. EN 1996-1-2 that presents guidelines for

[1] https://www.openstreetmap.org/.
[2] https://www.urbano.io/.
[3] https://github.com/ladybug-tools/lbt-grasshopper-samples/tree/master/samples/dragonfly.
[4] https://www.rhino3d.com/.
[5] https://github.com/BehnamMohseniGharyehsafa/buildingCommunityEnergyFlowSimulation.
[6] https://energyplus.net/.
[7] https://github.com/urbanopt/urbanopt-cli.

Table 1
Summary of the building envelope standards, Irish standards (I.S.) codes, and their applications.

Standards and codes	Application
I.S. 325 [47]	Masonry wall construction
I.S EN 1996 (Eurocode 6) [48]	Design and structural guidance for masonry
I.S. EN 1996-1-1 [48]	Masonry wall structural and reinforcement design
I.S. EN 1996-1-2 [48]	Fire safety for masonry walls
I.S. EN 1996-2 [48]	Material section and construction methods for masonry
I.S. 440 [49]	Concrete wall construction design and execution
I.S. 189 [50]	Structural concrete elements in walls
I.S. 401 [51]	Timber frame wall construction
I.S. EN 1365 [52]	Fire resistance evaluation of walls

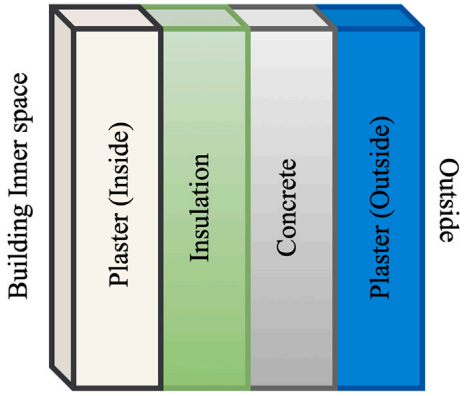

Fig. 3. Typical Irish wall structure for building envelope [53].

the structural fire design to ensure that the masonry walls comply with fire resistance requirements, and the I.S. EN 1996-2 that provides guidelines for the selection of materials and execution of masonry, resulting in covering the specification of materials and construction methods [48].

The I.S. 440 is relevant to the wall constructions involving concrete materials in the walls and thereby highlights the guidelines for proper design, materials, and workmanship in the concrete construction of the walls [49]. Additionally, the I.S. 189 code of practice for the structural use provides guidelines for the elements essentials for the concrete [50]. The I.S. 401 and I.S. EN 1365 codes of practice offer essential guidelines for the design, materials, and construction of timber-framed walls [51], as well as for determining the fire resistance of load-bearing walls [52]. Table 1 summarizes the I.S. standards and their applications.

Following the NSAI code of practice, we categorize the building wall constructions into four templates and this is presented in Fig. 3 [53]. The first and second categories consist of utilizing the plaster at the inside, bricks, insulation layer, and then plaster at the outside [54]. The third category is made of plaster (inside), cavity blocks, insulation layer, and plaster (outside), while the fourth category consists of plaster on the inside, the bricks, insulation layer, bricks, and then plaster on the outside. Since it was estimated that about 44 % of wall constructions in Ireland fall under the first category configuration [55], this work mainly investigates and considers this configuration as the foundation. A detailed configuration of the Irish wall materials based on the NSAI standards and various codes of practice is thus provided in the subsequent Table 2.

3.2.3. Heating, ventilation, and air conditioning system

In compliance with the NSAI standards for building and wall construction materials and configurations, this section presents a detailed configuration of the HVAC systems utilized in most of the Irish buildings. The developed HVAC system setup consists of three different configurations, including the gas boiler system, electric heater system, and the air-source-heat pump system in typical residential and commercial buildings of Ireland, as shown in Fig. 4 [56].

3.3. Establishment of Gaussian process for estimating the uncertainties

Gaussian process, inspired by Gaussian distribution, is a non-parametric data modeling technique employing a probabilistic approach for learning complex patterns [42]. The main difference between the Gaussian process and Gaussian distribution is that Gaussian distribution is applied to a vector of inputs and the observations, while the Gaussian process is applied to functions. This section presents the Gaussian process used in the current study to provide an estimation of the uncertainties associated with the model predicting the EUI for retrofitted buildings.

A Gaussian process is defined as a function (f), employing a Gaussian distribution of input vectors with the observations where for each new random variable, the output of the Gaussian process is the expected mean and the covariance of the new random independent variable. The mean (μ) of the random variable (x) is computed through the expectation of the x, as presented in Eq. (8). Likewise, the covariance (k) is the function of the two points x and x' of the random variable as presented in Eq. (9). Following Eqs. (8) and (9), we define the Gaussian process f, as presented in Eq. (10).

$$\mu(x) = \mathbb{E}[f(x)] \tag{8}$$

$$k(x, x') = \mathbb{E}[(f(x) - \mu(x))(f(x') - \mu(x'))] \tag{9}$$

$$f(x) = \mathcal{GP}(m(x), k(x, x')) \tag{10}$$

where $\mathbb{E}$ is the expectation of the random variable x. In most cases, for the sake of simplicity, the mean of the Gaussian process is assumed to be zero [57], leading to a joint normal distribution of covariance around the new random variable. We are interested in capturing the mean estimation of the new observation (e.g., new random variable). Assuming the input vectors $x = \{x_1, x_2, \cdots, x_m\}$ with the observations vector $f(x) = \{f(x_1), f(x_2), \cdots, f(x_m)\}$, the mean of observation for

Table 2
Characterization of the Irish building wall materials based on the National Standards Authority of Ireland (NSAI) [46].

Characteristics	Plaster board – 3/8 inch (Inner and Outer)	Concrete block wall	Wall insulation
Thickness [m]	0.0095	0.2032	0.0337
Thermal conductivity [W/m-K]	0.57	0.71	0.04
Density [kg/m3]	800	800	91
Specific heat [J/kg-K]	1089.29	831.46	836.46
Roughness	MediumSmooth	MediumSmooth	MediumSmooth
Thermal absorptance	0.9	0.9	0.9
Solar absorptance	0.7	0.7	0.7
Visible absorptance	0.7	0.7	0.7

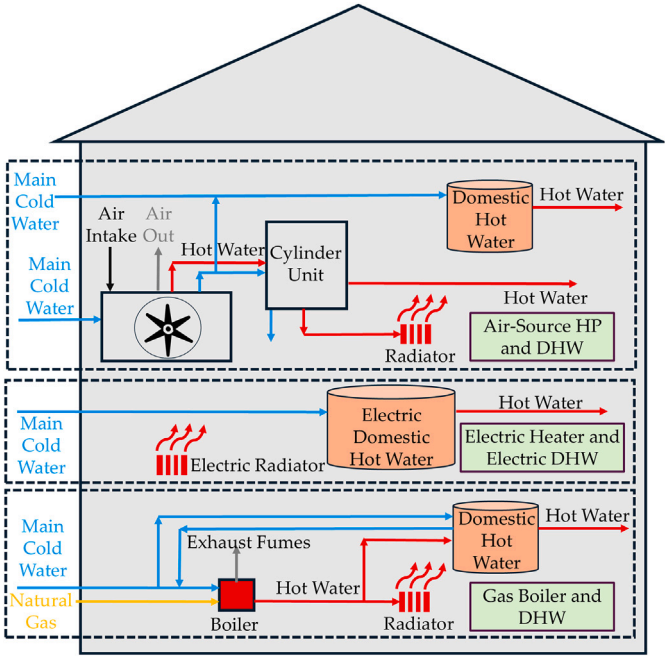

Fig. 4. A representation of the heating, ventilation, and air conditioning (HVAC) systems, highlighted different configurations for the gas (gas boiler and domestic hot water (DHW) system), electric (electric heater and electric DHW system), and heat pump (air-source heat pump (HP) and DHW system) settings.

a new vector of random variables $x_* = \{x_*^1, x_*^2, \cdots, x_*^m\}$ is estimated through Eq. (11) [58].

$$\begin{bmatrix} f(x_1) \\ \vdots \\ f(x_m) \\ f(x_*^1) \\ \vdots \\ f(x_*^m) \end{bmatrix} = \mathcal{N}\left(0, \begin{bmatrix} \mathcal{K}(x,x) & \mathcal{K}(x,x_*) \\ \mathcal{K}(x_*,x) & \mathcal{K}(x_*,x_*) \end{bmatrix}\right) \tag{11}$$

where $\mathcal{K}$ represents the kernel function, which is used to calculate the covariance of the vector of new independent variables. In our work, we utilized radial basis function (RBF) as of the kernel in Eq. (12) [59].

$$\mathcal{K}(x,x') = \exp\left(-\frac{\|x-x'\|^2}{2l^2}\right) \tag{12}$$

where l shows the spread of the kernel. To fine-tune all the hyperparameters, the log marginal likelihood function is used to find the optimum value of the parameters for the most suitable training. In the Gaussian process, the marginal likelihood function is the likelihood of the observation in the training (i.e., prior) phase of the Gaussian process. Given that the marginal likelihood has a small value, therefore logarithm of this function is used as presented in Eq. (13) [43,60].

$$\log p(Y|X,\theta) = -\frac{1}{2}Y^T\mathcal{K}^{-1}Y - \frac{1}{2}\log|\mathcal{K}| - \frac{n}{2}\log 2\pi \tag{13}$$

where Y is the vector of the training observations, X is the training independent vector, θ represents the kernel hyperparameters, and n is the number of the training instances. In Eq. (13), the first term $\left(-\frac{1}{2}Y^T\mathcal{K}^{-1}Y\right)$ shows the gain for the fitting, while the second $\left(-\frac{1}{2}\log|\mathcal{K}|\right)$ term shows the penalty for the overfitting. The last term $\left(-\frac{n}{2}\log 2\pi\right)$ represents a constant normalization function. Considering the maximization of the log marginal likelihood, the optimum hyperparameter (e.g., optimal variances, noise level, bandwidth level, etc.) that represents the pattern of the data can be obtained. Consequently, the mean function ($\overline{f(x_*)}$) and the covariance function ($\mathrm{Cov}(f(x_*))$) of the new random variables can be computed according to Eq. (14).

$$\begin{cases} \overline{f(x_*)} = \mathcal{K}(x_*,x)\mathcal{K}^{-1}(x,x)f(x) \\ \mathrm{Cov}(f(x_*)) = \mathcal{K}(x_*,x_*) - \mathcal{K}(x_*,x)\mathcal{K}^{-1}(x,x)\mathcal{K}(x,x_*) \end{cases} \tag{14}$$

where $\mathcal{K}(x_*,x)$ is the kernel covariance of the new variable with the previous, $\mathcal{K}^{-1}(x,x)$ is the inverse of the kernel covariance of previous variables, $\mathcal{K}(x_*,x_*)$ is the kernel covariance of the new variables, and $\mathcal{K}(x,x_*)$ is the kernel covariance of the previous input data with the new random variables. Following the mean and covariance functions of the new variable x_*, the uncertainty estimation discussed in Eq. (5), is computed based on the input data X, as presented in Eq. (15).

$$\hat{\sigma}_{GP}(x_*) = \sqrt{k(x_*,x_*) - k(x_*,X)k(X,X)^{-1}k(X,x_*)} \tag{15}$$

The uncertainty estimated in Eqs. (5) and (15) and the $\widehat{EUI}_{DL}$ computed through Eq. (6) are coupled through the developed GPDL discussed in Eq. (7) to evaluate the $\widehat{EUI}$.

3.4. Calculation of the primary energy sources for energy community

The specific primary energy sources (SPES) are the naturally occurring forms of resources (e.g., coal, crude oil, natural gas, solar, wind, biomass, geothermal, etc.), which are used to generate electricity, heat, or/and other forms of energy for human use [61]. Therefore, these energy sources are usually considered the starting point of the energy supply chain [62]. The SPES consumption is a fundamental element used to determine the energy costs for end-user consumption [63]. However, there are marginal cost factors (e.g., extraction difficulty, the efficiency of energy conversion, market fluctuations, and environmental regulations) that contribute to the final cost of energy for the end-user community [64], as presented in Fig. 5.

The figure portrays that the final energy is the energy available to consumers (e.g., gas at the burner tip or the electric energy obtained from plugs) with the marginal cost of losses occurring during transmission line constraints and step-up and step-down processes, resulting in influencing the final cost factor. This implies that SPES consumption is directly associated with the final energy costs meaning that the higher the SPES, the more the energy community has to bear the cost of their consumption. Consequently, determining the SPES consumption for the end-user energy community that results in reducing the final cost of electricity, heating, and transportation, is one of the fundamental goals of energy policymakers. To determine the SPES consumption and its implications on the energy cost for the end-user energy community, we define the PEF as the ratio of the SPES consumption to the EUI estimated through the GPDL, as presented in Eq. (16). This establishment aims to support the energy sector and policymakers in accurately determining the SPES consumption for each of the SPES and allocating specific SPES such as some of the user's energy being fed through natural sources (e.g., natural gas), while others may be suitable to be connected to the RESs, and thereby support the lowering of the overall energy cost.

$$PEF = \frac{SPES_{consumption}}{EUI} \tag{16}$$

The PEF indicates the consumption of the SPES such as a $PEF > 1$. This means that more energy is consumed due to the inefficiency of the conversion process, losses, and an inefficient energy supply chain that provides the final energy; resulting in a higher energy cost for the end-user energy community. The PEF offers a comprehensive scale by considering the upstream and downstream energy losses and the energy footprint of an energy carrier, from the SPES to end-use energy community applications. In several countries including the Republic of Ireland (ROI), the PEF is used in practice for energy rating certificates and building codes to provide an equitable comparison for the energy

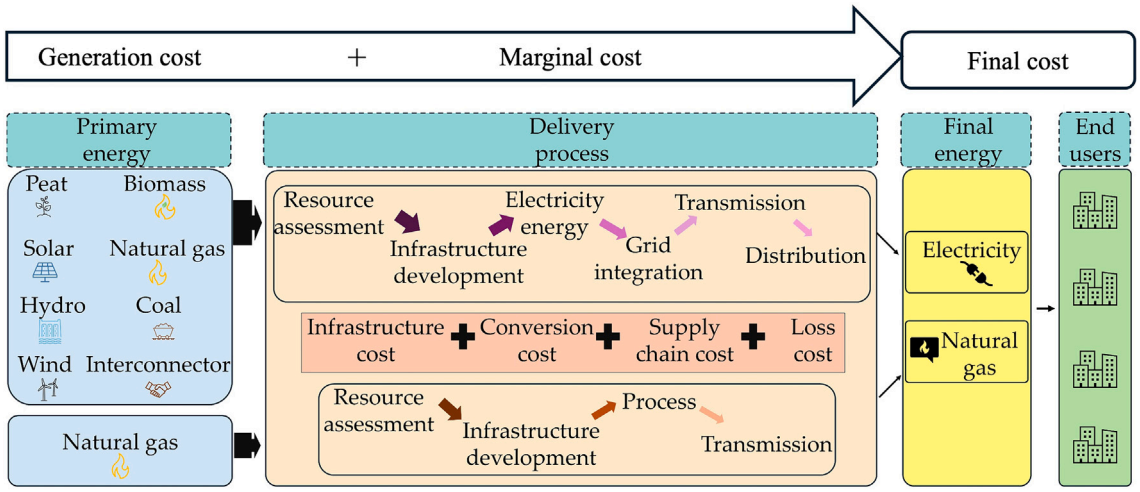

Fig. 5. An illustration of the energy cost for the end-user energy community, highlighting the generation and marginal cost factors contributing to the final energy cost.

Table 3
Characterization of the Primary Energy Factor (PEF) for various renewable and non-renewable energy sources [65].

Fuel type	Fuel utilized	PEF		Total PEF
		Renewable	Non-Renewable	
Gas	Main Gas	0	1.1	1.1
	Bulk LPG (propane or butane)	0	1.1	1.1
	Bottled LPG	0	1.1	1.1
Oil	Heating oil	0	1.1	1.1
	Biodiesel from renewable sources only	1	0.3	1.3
	Bioethanol from renewable sources only	1	0.34	1.34
Solid Fuel	House coal	0	1.1	1.1
	Anthracite	0	1.1	1.1
	Manufactured smokeless fuel	0	1.2	1.2
	Peat briquettes	0	1.1	1.1
	Sod peat	0	0.1	0.1
	Wood logs	1	0.1	1.1
	Wood pellets – in bags, for secondary heating	1	0.1	1.1
	Wood pellets – bulk supply, for main heating	1	0.1	1.1
	Wood chips	1	0.1	1.1
	Solid multi-fuel	0	1.1	1.1
District Heating Schemes	Heat from boilers – waste combustion	0	1.1	1.1
	Heat from boilers – waste combustion	0	1.05	1.05

carriers used to run the heating and cooling in buildings and is therefore predefined as provided in Table 3.

This implies that for the given predefined PEF (i.e., Table 3) for a fair comparison among the various SPES consumption, the estimation of the EUI plays a crucial role for the energy sector and policymakers to identify and allocate the most suitable SPESs to the energy communities that result in lowering the marginal costs. Therefore, our contribution of accurately estimating the EUI based on the GPDL has a critical role for the energy sectors and the policymakers. Given electricity and gas as the two dominant SPES in Ireland, their total energy consumption including the marginal energy can be calculated according to Eq. (17).

$$SPES_{consumption} = \widehat{EUI} \times PEF_s \quad \text{for } s = \{E, G, \cdots, O\} \tag{17}$$

where s represents the SPES such that E is electricity, G is the gas source, and O is the other sources (i.e., peat, biomass, RESs, etc.).

In order to compute the energy consumption, in the subsequent section we estimate the EUI based on the developed GPDL and present the overall process in the pseudocode of the proposed approach.

3.5. Pseudocode of the proposed GPDL

The proposed GPDL is developed through a modular approach and is presented in Algorithms 1 and 2. The main Algorithm starts 1 and utilizes the services of Algorithm 2 by performing the following main steps.

Step 1. Initialize the loop control variables ($i = 1$, $j = 1$), and $t = 1$, such that i, j, and t represent the indices for the building, the number of energy devices, and the time, respectively;

Step 2. For each of the ith buildings, iterate through all of their energy devices (j). Likewise, for each of the jth energy devices, get their energy consumption at the time step (t) and aggregate the energy utilization in the time domain, considering the energy consumption in the previous time step ($t-1$) and the consumption in the current time step (t), following Eq. (2). Save their energy utilization in the history variable for energy consumption (E_h). Check the time against the maximum time (T) for each of the jth devices and repeat until the maximum time for all the energy devices (n);

Step 3. Get the area (A_j) for each of the buildings and calculate the end-use-intensity (EUI_j) for each of the buildings following Eqs. (1)

Algorithm 1 Main Algorithm for acquiring the specific primary energy source (SPES) consumptions based on the end use intensity (EUI) estimation.

Initialize system parameters
for ($i = 1$ to N) **do** ▷ *Iterate through each building*
  while ($t \leq T$) **do**
    $\text{Temp}_1 \leftarrow E_t$
    $\text{Temp}_2 \leftarrow E_{t-1}$
    for ($j \leq n$) **do** ▷ *Iterate through energy device*
      if ($\text{Temp}_1 != 0$ && $\text{Temp}_2 != 0$) **then**
        $E_j \leftarrow \text{Temp}_1 + \text{Temp}_2$
        $Temp_3 \leftarrow A_j$
        $E_h \leftarrow E_j$
        $EUI_j \leftarrow \frac{E_j}{\text{Temp}_3}$ ▷ *Calculate the EUI*
        $EUI_h \leftarrow EUI_j$
        $A_h \leftarrow \text{Temp}_3$
      end if
      $j \leftarrow j + 1$
    end for
    $t \leftarrow t + 1$
    $\text{Temp}_1 \leftarrow 0$
    $\text{Temp}_2 \leftarrow 0$
  end while
  $i \leftarrow i + 1$
  $\text{Temp}_3 \leftarrow 0$
end for
$\widehat{EUI} \leftarrow GPDL(E_h, A_h, EUI_h)$ ▷ *Call algorithm 2*
while ($s \leq S$) **do** ▷ *Calculate PES consumption*
  $PES_s \leftarrow \widehat{EUI} \times PEF_s$
  $s \leftarrow s + 1$
end while
Print the results

and (3). Save the calculated EUI_j and the A_j for the jth building into their corresponding historical variables EUI_h and A_h and iterate through each of the buildings until all the N buildings in the smart city;

Step 4. Call Algorithm 2 by passing the energy, building area, and end-user-intensity parameters. Algorithm 2 optimizes predictions of EUI through the process of the GPDL framework by following these main steps:

4.1. Perform the initialization of the system parameters, including the input, output, and loop control variables, and prepare the input feature matrix (X) and target variable (Y), such that the matrix x consists of energy consumption and the building area characteristics, while the output is considered to be the end-user-intensity. Consequently, split the dataset into the train-test datasets with 80 % and 20 %, respectively;

4.2. Characterize the kernel by initializing a range of length scales and noise level hyperparameters for tuning the Gaussian Process model. Consequently, for each hyperparameter, construct a combined kernel using the constant kernel (Ck), radial basis function (RBF), and white kernel (W) to capture both the smooth and noisy variations in the data points;

4.3. Initialize the GPR model with the constructed kernel to identify the uncertain data points, predict the target variable by training the dataset, and calculate the prediction accuracy (RMSE). Subsequently, depending on the RMSE iteratively performs hyperparameter tuning to identify the uncertain data point and thereby find the optimal kernel parameters. If there is an improvement in lowering the RMSE, store it as the best kernel parameter;

4.4. Initialize the DL with the optimal kernel obtained through the GPR resulting in the GPDL model. Predict the EUI based on the developed GPDL model, compute the RMSE, and return the optimized prediction and its corresponding accuracy (RMSE) to the main Algorithm 1.

Step 5. Iterate through each of the primary energy sources and compute the SPES consumption based on the estimated EUI and the given PEF;

Step 6. Print the corresponding results and exit the algorithm.

4. Simulation setup and results discussion

4.1. Description of the mullingar case study

The proposed GPDL model is tested on a case study conducted in Mullingar City, a town in County Westmeath, Ireland. The population of Mullingar City is more than 22,000 with an elevation level of 101 meters according to the 2022 [66] survey. The case study considers a total of 6076 buildings consisting of a wide range of mixed building types from Mullingar City and the suburban areas. The perspective geographical view of Mullingar is shown in Fig. 6. A characterization of the operations of the various building types including residential, commercial, industrial, public & government, religious, recreational & entertainment, transportation & infrastructure, cultural & historical, and specialty, along with the number of constructions and the gross floor area, is tabulated in Table 4.

4.2. Simulation setup

The proposed GPDL model is developed by leveraging a feedforward neural network (FNN) in Python 3.12.1, running on a system with a 13th Gen Intel (R) Core (TM) i9-13900, 24 logical cores, 64 GB of RAM with a speed of 4400 MHz, and 40 GB of Cached. A detail of the simulation environment is presented in Table 5.

4.3. Performance evaluation criteria

To ensure the credibility of the proposed GPDL model, several different performance criteria are utilized including error analysis, bias detection, model fit, model complexity and selection, residual assessments, uncertainty, predictive distribution, benchmarking, and relative performance. The performance analysis criteria are based on various performance metrics and are presented in the subsequent subsections.

4.3.1. Error analysis

The error analysis incorporates performance metrics that analyze the model's performance by evaluating the difference between the true values and the predicted values for each of the data points. The results highlight that a minimum and larger difference represents the model's ability and inability to understand the data pattern. Consequently, the error analysis utilizes the following performance metrics.

1. *Mean Squared Error:* The mean squared error (MSE) evaluates the average squared difference between the actual and predicted data points and quantifies that a lower value of the MSE indicates that the model predictions are closer to the actual data points, while a higher MSE showcases a larger margin between the two data points and is thus regarded as poor performance of the model, as presented in Eq. (18). A variation of the MSE is the root mean squared error (RMSE) that takes the square root of the MSE to make the units compatible with the corresponding target variable for analyzing the model performance in more interpretable, real-world terms, as presented in Eq. (19) [67].

Algorithm 2 GPDL (E_h, A_h, EUI_h)

Inputs: E_h, A_h, EUI_h
Output: Optimized predicted (EUI), Prediction accuracy ($RMSE$)

Initialize all the system parameters
$X \leftarrow [E_h, A_h]$ ▷ *Prepare feature matrix*
$Y \leftarrow EUI_h$ ▷ *Prepare target values*
$X_{\text{train}}, X_{\text{test}}, Y_{\text{train}}, Y_{\text{test}} \leftarrow \text{train\_test\_split}(X, Y, \text{test\_size} = 0.2)$ ▷ *Split the dataset*
$L_{\text{scale}} \leftarrow \text{linspace}(0.1, 2.0, 10)$ ▷ *Initialize kernel length scales*
$N_{\text{levels}} \leftarrow \text{logspace}(-3, 0, 10)$ ▷ *Initialize noise levels*
$RMSE_{\text{updated}} \leftarrow \infty$ ▷ *Initialize best RMSE*
for each l in L_{scale} **do** ▷ *Optimize kernel's hyperparameters*
  for each n in N_{levels} **do** ▷ *Define combined kernel*
    $C_k \leftarrow C(1.0, (1\text{e-}3, 1\text{e}3))$
    $RBF_k \leftarrow \text{RBF}(\text{length\_scale} = l)$
    $W_k \leftarrow \text{WhiteKernel}(n_{\text{level}} = n, n_{\text{level\_bounds}} = (1\text{e-}5, 1\text{e}1))$
    $kernel \leftarrow C_k \times RBF_k + W_k$ ▷ *Combine kernel parameters for optimization*
    $GP_{\text{EUI}} \leftarrow \text{GPR}(kernel, \text{optimizer})$ ▷ *Initialize GPR model for EUI*
    $\widehat{\text{EUI}} \leftarrow GP_{\text{EUI}}(X_{\text{train}}, Y_{\text{train}})$ ▷ *Train the model*
    $RMSE_{\text{EUI}} \leftarrow \sqrt{\text{MSE}(Y_{\text{train}}, \widehat{\text{EUI}})}$ ▷ *Calculate RMSE for EUI*
    if $RMSE_{\text{EUI}} \leq RMSE_{\text{updated}}$ **then** ▷ *Update the best RMSE*
      $RMSE_{\text{updated}} \leftarrow RMSE_{\text{EUI}}$
      $best\_kernel\_eui \leftarrow kernel$
$GPDL_{\text{EUI}} \leftarrow \text{GP}(best\_kernel\_eui, \text{optimizer})$ ▷ *Optimized GPR model*
$\widehat{\text{EUI}}_{\text{updated}} \leftarrow GPDL_{\text{EUI}}(X_{\text{train}}, Y_{\text{train}})$ ▷ *Train the optimized hybrid model following Eq. (7)*
$RMSE_{\text{EUI}_{\text{updated}}} \leftarrow \sqrt{\text{MSE}(Y_{\text{train}}, \widehat{\text{EUI}}_{\text{updated}})}$
Return $\left(\widehat{\text{EUI}}_{\text{updated}}, RMSE_{\text{EUI}_{\text{updated}}}\right)$ ▷ *Return the results*

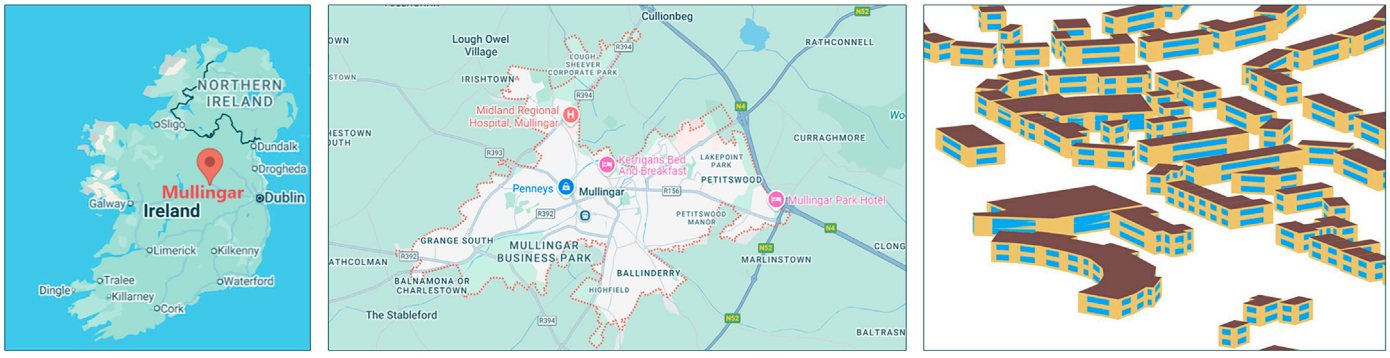

Fig. 6. A representation of the Mullingar aerial view and building information modeling.

$$\text{MSE} = \frac{1}{n}\sum_{i=1}^{n}(y_i - \hat{y}_i)^2 \tag{18}$$

$$\text{RMSE} = \sqrt{\frac{1}{n}\sum_{i=1}^{n}(y_i - \hat{y}_i)^2} \tag{19}$$

$$\text{CV-RMSE} = \left(\frac{RMSE}{\bar{y}}\right) \times 100 \tag{20}$$

$$\text{R-RMSE} = \begin{cases} \left(\frac{RMSE}{\max(y_i) - \min(y_i)}\right) \times 100 & \text{Range as reference} \\ \left(\frac{RMSE}{\sigma_y}\right) \times 100 & \text{Std. as reference} \end{cases} \tag{21}$$

The Coefficient of Variation of RMSE (CV-RMSE) and the Relative Root Mean Squared Error (R-RMSE) are versions of the normalized variations of the RMSE [68]. The CV-RMSE measures the normalized mean of the observed data, as presented in Eq. (20) [69], while the R-RMSE variant is normalized by a reference range and the standard deviation associated with the true data points, as presented in Eq. (21) [70]. Both the CV-RMSE and R-RMSE variants are represented as percentages, highlighting that larger values indicate poor performance while smaller values indicate better performance of the model.

2. *Mean Absolute Error:* The Mean Absolute Error (MAE) represents a measurement of the average absolute difference between the predicted data points and the actual data points as presented in Eq. (22) [71]. The MAE is more robust to outliers compared to the MSE and RMSE as in the latter two cases squaring the errors means that larger errors have a disproportionately larger impact on the final error outcome [72].

$$\text{MAE} = \frac{1}{n}\sum_{i=1}^{n}|y_i - \hat{y}_i| \tag{22}$$

Table 4
A characterization of buildings information classified by the building types for the Mullingar case study.

Building type	Building name	Number of constructions	Total gross floor area [m^2]
Commercial	Bank	3	2493.75
	Beauty saloon	1	37.79
	Bicycle store	1	145.92
	Bookmaker store	1	124.85
	Book store	1	696.13
	Café	3	440.23
	Car part store	1	2591.13
	Car rental	1	259.04
	Car store	4	2650.85
	Clothes store	4	523.39
	Convenience store	1	309.06
	Florist	1	74.46
	Hardware store	2	1031.94
	Insurance office	2	346.04
	Jewelry store	2	150.78
	Optician store	1	229.59
	Restaurant	2	284.25
	Supermarket store	7	12804.09
	Variety store	1	2043.4
Public and government	Community center	2	4082.16
	Courthouse	1	1906.96
	Governmental	1	1472.65
	Library	2	3274.04
	Police station	1	1945.19
	Post office	1	972.6
	Public toilet	2	106.3
	Townhall	1	1517.27
	Clinic	1	510.58
	Dentistry	2	207.6
	Kindergarten	1	433.56
	Outpatient	2	1219.0
	Pharmacy	2	798.6
	School	1	852.26
	Art center	1	3225.29
Recreational and entertainment	Cinema	1	3910.85
	Nightclub	1	678.61
	Pub	8	1731.83
Transportation and infrastructure	Gas station	1	477.15
Specialty	Mortuary	1	478.41
Religious	Place of worship	5	5572.98
Residential	Residential buildings	5997	2.5263e+6

Table 5
A summary of the configuration parameters for deep retrofitting.

Category	Parameters name	Configuration details
Hardware	GPU	NVIDIA® T1000 8GB GDDR6 50.0 W Bus 128 bits Micron® Intel® UHD Graphics 770 Raptor Lake GT 10 nm
	CPU	13th Gen Intel® Core(TM) i9-13900 2.00 GHz
	Memory (RAM)	64 GB DDR5
	Storage	8 TB SSD
Software	Python	3.12.1
	EnergyPlus	23.2
	OpenStudio	3.7
	Ladybug Tools	1.84
	URBANopt	0.12.0
Platform	Operating System	Windows

The Mean Absolute Percentage Error (MAPE) and Symmetric MAPE (S-MAPE) are variations of the MAE [73]. The MAPE measures the absolute percentage error between the predicted and actual data points, as presented in Eq. (23) [74]. The S-MAPE measures the asymmetry between the overestimates and underestimates due to the bias caused by larger errors due to the limited actual data points, as presented in Eq. (24) [75].

$$\text{MAPE} = \frac{1}{n}\sum_{i=1}^{n}\left|\frac{y_i - \hat{y}_i}{y_i}\right| \times 100 \tag{23}$$

$$\text{S-MAPE} = \frac{1}{n}\sum_{i=1}^{n}\frac{|y_i - \hat{y}_i|}{\left(|y_i| + |\hat{y}_i|\right)/2} \times 100 \tag{24}$$

4.3.2. Bias detection

Bias is a systematic distortion error introduced by deep learning models during their training process while approximating the dependent variables. This can lead to unfair decision-making, commonly referred to as model over or under predictions. To identify the model bias, the mean bias error (MBE) is utilized, which measures the average bias in

the regression model and quantifies whether the model is overpredicting or underpredicting as presented in Eq. (25) [76].

$$\mathrm{MBE} = \frac{1}{n}\sum_{i=1}^{n}(\hat{y}_i - y_i) \tag{25}$$

The MBE criteria provide a tool to understand the direction of the error, providing a consolidated diagnosis of overestimation and underestimation of the model to enhance the model's precision. A positive value of MBE shows that the model is overpredicting the results, the negative sign shows that regression is underpredicting, and the zero value shows a neutral unbiased system [77].

4.3.3. Model fitting

Model fitting is a criterion that refers to the relationship between the input features (independent variables) and the output feature (dependent variable) [78]. A closer fit means a well-established relation leading to an output closer to the true features. There are several performance metrics that provide model-fitting measurements, such as R-squared score and index of agreement, which are presented below.

1. *R-Squared Score:* The R^2 score measures the variation of the dependent variables from the independent variables. The criterion is established by subtracting the sum of squares of residuals from the total sum of squares with the unit, as presented in Eq. (26) [79]. The value of R^2 close to the unit indicates that a large proportion of the variance of the results is well-explained by the model, an R^2 value close to zero implies a poor prediction performance of the model.

   A modified version of the R^2 that considers penalty factor for the added variables that do not enhance the model notably; usually leading the model to be overfitted, as presented in Eq. (27) [80]. This criterion is useful for the models with numerous predictors and aims to have a model with strength in explanatory power while keeping the complexity as low as possible.

$$\mathrm{R}^2 = 1 - \left[\frac{\sum_{i=1}^{n}(y_i - \hat{y}_i)^2}{\sum_{i=1}^{n}(y_i - \bar{y})^2}\right] \tag{26}$$

$$\text{Adjusted } \mathrm{R}^2 = 1 - \left[\frac{(1 - R^2)(n-1)}{n - p - 1}\right] \tag{27}$$

   The denominator $(n - p - 1)$ penalizes the adjusted R^2 for the number of predictors, with n being the total number of observations and p being the independent variables (predictors) included in the model.

2. *Index of Agreement:* The Index of Agreement (d_1) evaluates the performance of the predictive model by assessing both the magnitude and the direction of the error to determine how well the predicted value from the regression model matches with the observed value as presented in Eq. (28) [81].

$$\mathrm{d}_1 = 1 - \left[\frac{\sum_{i=1}^{n}(y_i - \hat{y}_i)^2}{\sum_{i=1}^{n}(|y_i - \hat{y}_i| + |y_i - \bar{y}|)^2}\right] \tag{28}$$

   Given the complex nature of building mechanical and thermodynamic architectural points, capturing the energy flow inside the building requires a careful understanding of the interaction between multiple diverse factors. Consequently, the index of agreement plays a crucial role in measuring the ability of the complex energy pattern.

4.3.4. Model complexity

The number of parameters and their corresponding relationships contribute to the complexity of the model and serve as evaluation criteria for the model's generalization. A highly complex model may meet the model fitting criterion during the training process; however, there is a risk of performance degradation on unseen datasets. Therefore, a well-developed model should strike a balance between complexity for both training and generalization purposes. To measure model complexity we use the Akaike information criterion (AIC) and Bayesian information criterion (BIC) mechanisms [82].

The AIC measures the number of parameters and their maximum likelihood for balancing goodness of fit and model complexity by penalizing models that use more parameters to avoid overfitting, as presented in Eq. (29) [83]. Likewise, the BIC also focuses on the balance between goodness and model complexity; however, it penalizes the complexity more heavily to avoid overfitting, as presented in Eq. (30) [84].

$$\mathrm{AIC} = 2\left(k' - \ln(L)\right) \tag{29}$$

$$\mathrm{BIC} = k' \times \ln(n) - 2\ln(L) \tag{30}$$

where k' is the number of parameters and L is the maximum likelihood of the model.

4.3.5. Residuals assessments

To assess the performance and validity of regression models, the assessment of the important evaluation criteria is crucial. Residuals represent the differences between the observed and predicted data points. If residuals exhibit a pattern, it indicates that the model is failing to capture the estimated relationship between the variables. On another note, if the distribution of the residuals varies with the predicted data points instead of having a constant variance, it results in heteroscedasticity [85].

Residuals assessment can be analyzed through the Shapiro–Wilk test and p-value to evaluate the normality of the residuals and the Quantile–Quantile (Q-Q) plot to qualitatively analyze the distribution of the residuals and further assess their normality [86]. The Shapiro–Wilk Test determines whether the residuals from a model follow a normal distribution based on the number of observations and their corresponding sample mean, as presented in Eq. (31).

$$\mathrm{W} = \frac{\left[\sum_{i=1}^{n} a_i x_{(i)}\right]^2}{\sum_{i=1}^{n}(x_i - \bar{x})^2} \tag{31}$$

where x is the number of the observations, x_i is the i-th observation in the sample, $\bar{x}$ is the sample mean, $x_{(i)}$ is the order statistics from smallest to largest, and α_i is the weight obtained from the expected value of the observations, standard normal distribution, and the covariance matrix. When the value of W is close to 1, the sample data seem to be normally distributed, and when the value of W is notably smaller than 1, this indicates that the data are not normally distributed.

The p-value helps to interpret the results of the Shapiro–Wilk test indicating whether to reject the assumption of normality [86]. A high p-value (p-value > 0.05) indicates that there is no significant evidence against the normality of residuals, leading to the consideration of residual normality. On the other hand, a low p-value (p-value ≤ 0.05) indicates that the residuals deviate significantly from a normal distribution. The Q-Q plot is a graphical tool that plots the percentiles of the experimental observations against the theoretical percentiles of a normal distribution to determine whether the sample of the dataset has a normal distribution or not, as presented in Eq. (32) [87].

$$\mathrm{Q_i} = \Phi^{-1}\left[\frac{i - 0.5}{n}\right] \tag{32}$$

where Q_i is the theoretical percentile, i is the rank of the data, n is the number of observations, and Φ^{-1} is the standard normal Cumulative Distribution Function (CDF) inverse.

4.3.6. Uncertainty handling

The uncertainty in the model arises from the variability in data, measurements, or parameters, restricting the model from making informed

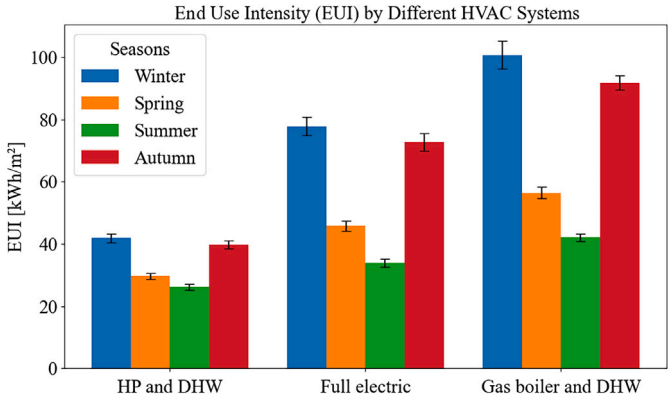

Fig. 7. Site end-use intensity comparison between different system configuration in the same envelope conditions for cold regions.

decisions. The predictive models are usually prone to aleatoric and epistemic uncertainties, such that the aleatoric uncertainty defines what exhibits from the variability and noise that exist in the dataset, while the epistemic uncertainty is related to the limited knowledge and parameters of the model. Two distinct criteria for this credibility angle are used, including prediction interval normalized average width (PINAW) and negative log predictive density (NLPD).

1. *Prediction Interval Normalized Average Width:* Prediction interval normalized average width [88] is the normalization of the average width of the prediction by the range of the true data, as presented in Eq. (33). A low PINAW shows the prediction intervals are around the true values, indicating predictions with low levels of uncertainty. A high value of PINAW indicates that the model performance is low.

$$\text{PINAW} = \frac{\sum_{i=1}^{n}(Upper_i - Lower_i)}{n \times (\max(y_i) - \min(y_i))} \tag{33}$$

2. *Negative Log Predictive Density:* Negative log predictive density (NLPD) is a criterion to evaluate probabilistic models using both the prediction and the associated uncertainty [89]. A low NLPD indicates a model with high probability density and high accuracy, while, high values of NLPD report on the poor performance of the model, as presented in Eq. (34). This evaluation criterion is useful for the models that represent a full predictive distribution by combining the magnitude of the error and the uncertainty.

$$\text{NLPD} = \frac{1}{n}\sum_{i=1}^{n}\left(\frac{(y_i - \hat{y}_i)^2}{2\sigma_i^2} + \frac{1}{2}\ln(2\pi\sigma_i^2)\right) \tag{34}$$

4.3.7. Relative performance

Comparing a model with benchmarks, like simple naïve models, can give a relative comparison of the true added value of using a model compared with a reference one. The criterion used to do this assessment is Theil's inequality coefficient (U-statistic) [90]. Theil's inequality coefficient is a relative measure that compares the RMSE of the model to the RMSE of a naïve model, the model that reveals the mean of the actual values, as presented in Eq. (35). A U-statistic close to zero indicates that the model has higher performance compared with the simple naïve one, while the U-statistic close to one shows that the usefulness and practicality of the model is under question and the performance is similar to the model that shows the mean of the values.

$$\text{U} = \frac{\sqrt{\frac{1}{n}\sum_{i=1}^{n}(\hat{y}_i - y_i)^2}}{\sqrt{\frac{1}{n}\sum_{i=1}^{n}\hat{y}_i^2} + \sqrt{\frac{1}{n}\sum_{i=1}^{n}y_i^2}} \tag{35}$$

4.4. Results discussion

4.4.1. Site end-use intensity

Three different HVAC systems, which are typical for the locality, are considered in this investigation. The systems are full electric space heating and domestic hot water, gas boiler and domestic hot water, and heat pump backed by domestic hot water. In the same envelope condition according to the cold climate conditions [91], the HVAC systems show different EUI results. The highest consumption is performed by gas boiler and DHW and the lowest is for the heat pump.

By changing the HVAC system of Mullingar City from a gas boiler to a heat pump, the EUI of the entire city decreases by 52.4 %. A fully electric HVAC system shares about 229.125 kWh/m2, and by changing the electric system to a heat pump, the city can save 39.2 % kWh energy by each square meter. Fig. 7 shows the difference between using a distinct HVAC system in Mullingar. According to Table 6, the system with a heat pump and gas boiler indicates the highest energy efficiency compared to the other systems for all the buildings in Mullingar, which is mostly because of the high efficiency of the heat pumps. This could be enhanced by integrating more renewable energy to feed the power grid.

4.4.2. Primary energy usage comparison

To compare different energy consumption scenarios, the source of the energy used should be equal to convey a fair and comprehensive analysis. This is more crucial for strategic policies impacting influential parameters on large scales like energy consumption and deep retrofit on community and urban scales. One of the criteria for making this comparison is the PEF. Primary energy indicates the energy found in a substance in nature that has not been processed by human activities, such as crude oil, coal, natural gas, solar, and wind. Final energy is the energy available to consumers after all the conversion, transmission, and losses, like the gas at the burner tip or the electric energy obtained from plugs.

The PEF offers a comprehensive scale by considering the upstream energy lost and the energy footprint of an energy carrier, from the source in nature to the end-use application. Various countries, including Ireland, employed the PEF to the energy rating certificates and building codes to have an equitable comparison for the energy carriers used to run the heating and cooling in buildings. To have a comparison between gas and electricity, two dominant sources of final energy for the end-users, electricity poses high PEF because of all the conversion from thermal to electricity regarding the associated losses.

In contrast, natural gas has a lighter upstream loss, resulting in lower PEF. The PEF factors for countries are different, related to the sources they used to supply the electricity grid. According to the reports [92,93], the PEF considering all the imports and exports in Ireland for electricity and natural gas is 1.75 and 1.1, respectively. Eq. (17) is used to calculate the primary energy use for each system in different periods. Note that each system has different loads such as heating, water system, HVAC

Table 6
Comparison of primary energy usage across different heating, ventilation, and air conditioning (HVAC) systems in Mullingar City, Ireland.

Period	HP and DHW EUI [kWh/m^2]	Full electric EUI [kWh/m^2]	Gas boiler and DHW EUI [kWh/m^2]
Spring	67.051	137.191	119.136
Summer	45.085	77.674	68.198
Fall	38.434	58.536	51.865
Winte	62.337	126.420	109.989
Annual	212.907	399.820	349.187

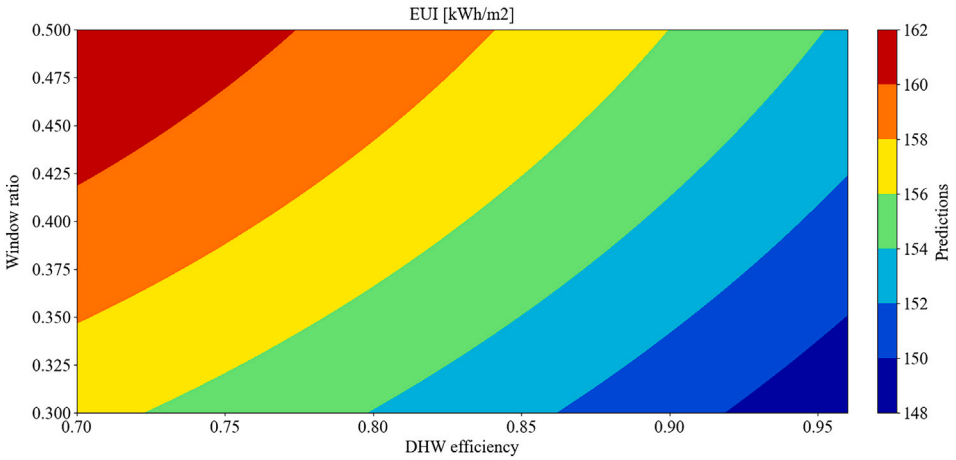

Fig. 8. Variation of domestic hot water (DHW) and window ratio to end use intensity (EUI).

fans, interior lighting, electric equipment, pump, and gas equipment. For each source in each system, the appropriate natural gas or electricity PEF should be used.

According to Table 6, the system with a heat pump and gas boiler indicates the highest energy efficiency compared to the other systems for all the buildings in Mullingar, which is mostly because of the high efficiency of the heat pumps. This could be enhanced by integrating more renewable energy to feed the power grid.

4.5. Data-driven deep retrofitting analysis

Since the heat pump shows much better performance and saves energy for cities according to the mentioned sensitivity, we use heat pump (HP) as the ideal HVAC system and we develop various retrofitting scenarios for the building envelope such as window ratio, DHW efficiency, and the number of insulation layer sandwiches in the exterior wall of Mullingar's city. Regarding the high number of buildings used in this investigation to have a much-consolidated representation of a real city, the simulations are time-consuming; each of them takes about 15 to 30 hours to get a prediction of annual EUI by using 24 cores of a high processing machine for a single case study.

To have rapid decision-making tools for urban planners and large-scale city construction, we developed for the first time a Gaussian Process of machine learning to simulate the annual end-use intensity. The Gaussian Process machine learning has two main advantages: (1) it is capable of handling the uncertainties due to its probabilistic approach, and (2) it shows promising results in managing data scarcity in complex problems [94]. The developed machine learning is highly precise with an RMSE of 3.24 and the model is capable of predicting the EUI in different window ratios from 30 % to 50 % of a side, distinct number of insulation from 1 to 5 layers, and DHW efficiency from 70 % to 95 %.

Fig. 8 shows the variation of EUI for different DHW efficiency and window ratio in default insulation of 3. In a fixed insulation layer, the variation of EUI with the DHW efficiency and window ratio is insignificant. To minimize energy use, a mixture of high DHW efficiency and lower window ratio is suggested. The importance of the insulation layer is shown in Fig. 9. With a fixed DHW efficiency of 0.8 and window ratio of 0.4, increasing the insulation layer from 1 to 3, 3.97 % decreases the EUI. Fig. 10 shows the variation of EUI versus insulation layer, and window ratio for 0.85 DHW efficiency. Enhancing the wall insulation from 1 to 5 layers, with a window ratio of 0.45, saves 7.93 % energy in each square meter in Mullingar.

4.6. Model performance

The credibility of the proposed GPDL model is evaluated against state-of-the-art linear regression [95] and spline regression [28] models and the results are analyzed following the performance evaluation criteria discussed in Section 4.3.

Table 7 (Error evaluation) portrays a remarkable performance with the proposed GPDL model achieving MSE and RMSE of 1.3005 $[kWh/m^2]^2$ and 0.0036 $[kWh/m^2]$, which is much smaller than that of linear and spline regression. The difference between the MSE of linear and spline regressions is about 0.5179 $[kWh/m^2]^2$, while the magnitude of the Gaussian process regression is in the order of 10 to 6. The order of magnitude of RMSE for the Gaussian process is 10 to 3, while the values for the linear and spline are 1.0760 $[kWh/m^2]$ and 0.8000 $[kWh/m^2]$. The RMSE criteria show that the Gaussian process model deviates about 0.0036 $[kWh/m^2]$ for the predictions. According to the order of magnitude of the results, the Gaussian process model shows an acceptable and accurate prediction.

In the case of MAE, the Gaussian process model has obtained the value of 0.0035 $[kWh/m^2]$. This means that on 'average', the prediction has an offset of about 0.0035 $[kWh/m^2]$. The MAE is lower than the RMSE, which means that larger errors do not inflate the error metrics; this indicates that even the highest order of magnitude of errors does not violate the credibility and accuracy of the model. However, linear and spline regressions show poor comparative performance. The spline regression's MAE is 0.5060 $[kWh/m^2]$ which is about half of the linear's values. The MAPE and S-MAPE of the linear regression are 0.6643 [%],

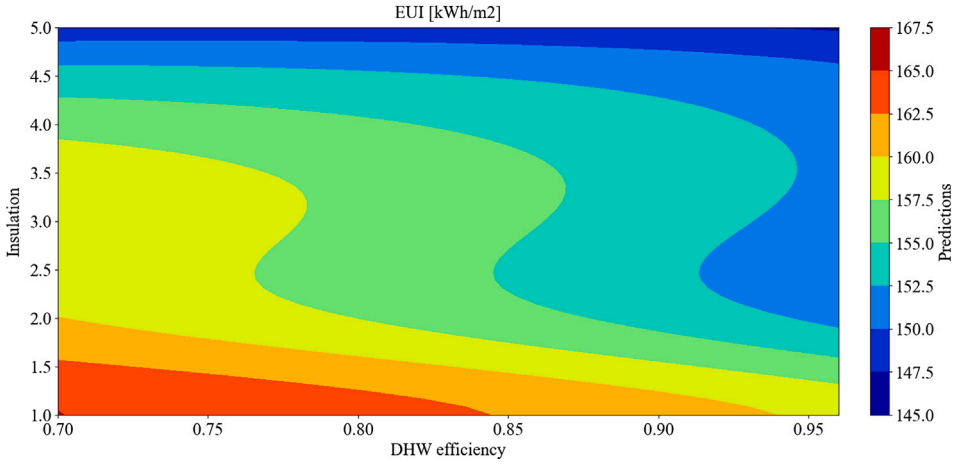

Fig. 9. Variation of domestic hot water (DHW) and number of insulation layer to end use intensity (EUI).

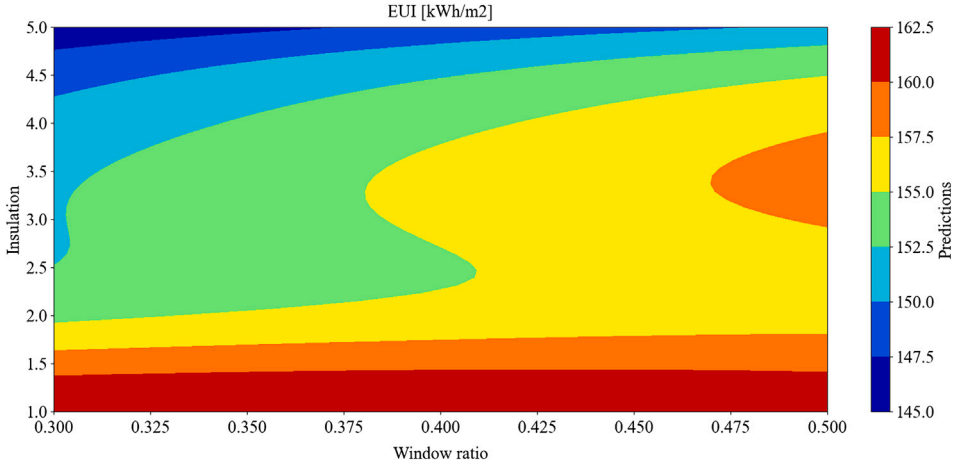

Fig. 10. Variation of number of insulation layer and window ratio to end use intensity (EUI).

Table 7
A comparison of the proposed Gaussian Process-based deep learning (GPDL) model with state-of-the-art linear and spline regression models using various performance evaluation criteria.

Criteria description	Performance metrics	Linear regression [27]	Spline regression [28]	Proposed GPDL
Error evaluation	MSE $[kWh/m^2]^2$	1.1579	0.6400	1.3005
	RMSE $[kWh/m^2]$	1.0760	0.8000	0.0036
	MAE $[kWh/m^2]$	1.0311	0.5060	0.0035
	MAPE [%]	0.6643	0.3310	0.0022
	S-MAPE [%]	0.6646	0.3309	0.0022
	CV-RMSE [%]	0.6905	0.5133	0.0023
	R-RMSE (Range-as reference) [%]	7.7023	5.7265	0.0258
	R-RMSE (Std. as reference) [%]	20.1901	15.0110	0.0676
Bias detection	MBE $[kWh/m^2]$	$-3.4106e^{-14}$	$-2.8421e^{-14}$	$-6e^{-4}$
Residual assessment	Shapiro–Wilk Test	0.8070	0.8834	0.8641
	p-value	0.0923	0.3254	0.2437
Uncertainty handling	PINAW	Not defined	Not defined	0.0008
	NLPD	Not defined	Not defined	−4.1871
Relative performance	U-statistic	$3.4e^{-3}$	$2.5e^{-3}$	$1.16e^{-5}$

and 0.6646 [%], respectively. These metrics are about 0.6621 [%] and 0.6624 [%] higher than the proposed GPDL results and are almost half of the spline.

The very narrow and close results of the Gaussian process show the excellence of the model prediction. The CV – RMSE of the proposed GPDL model is 0.0023 %, which implies that the RMSE is only about 0.002 % of the average predicted EUI. The low amount of the CV – RMSE indicates the highest precision of the model. However, the CV – RMSE of the spline and linear regression models is above 0.5 %. The RMSER (range as reference) of linear and spline regression models is 7.7023 % and 5.7265 %, respectively, while it is about 5.7 % lower than the proposed GPDL when compared to these state-of-the-art models. The RMSE (Std. as reference) of the proposed GPDL model is in the order of 10^{-2}% while for the spline and linear model is more than 15 %.

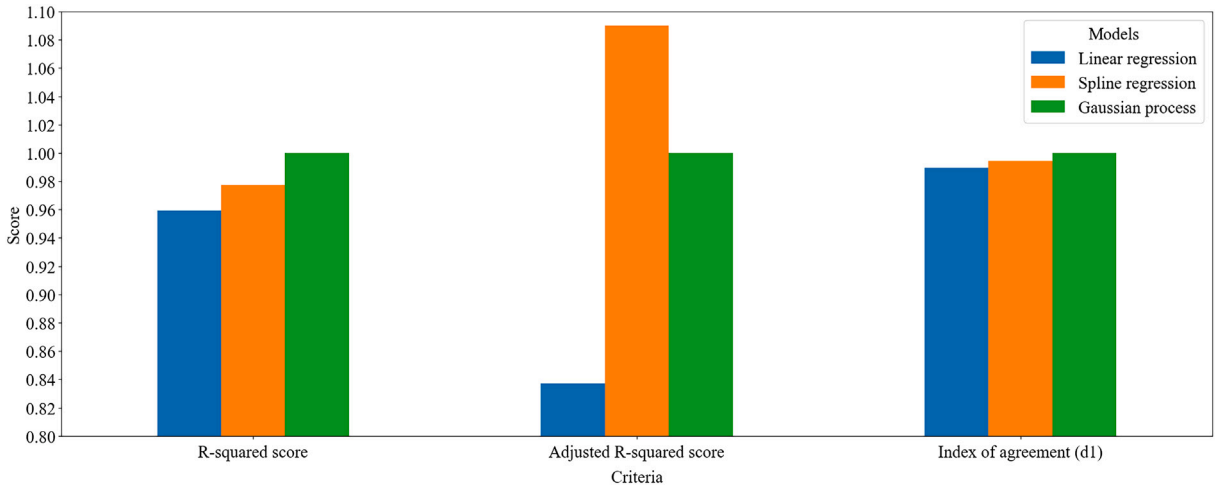

Fig. 11. A comparison of the model fit between the proposed Gaussian Process-based deep learning (GPDL) and the linear and spline regression models.

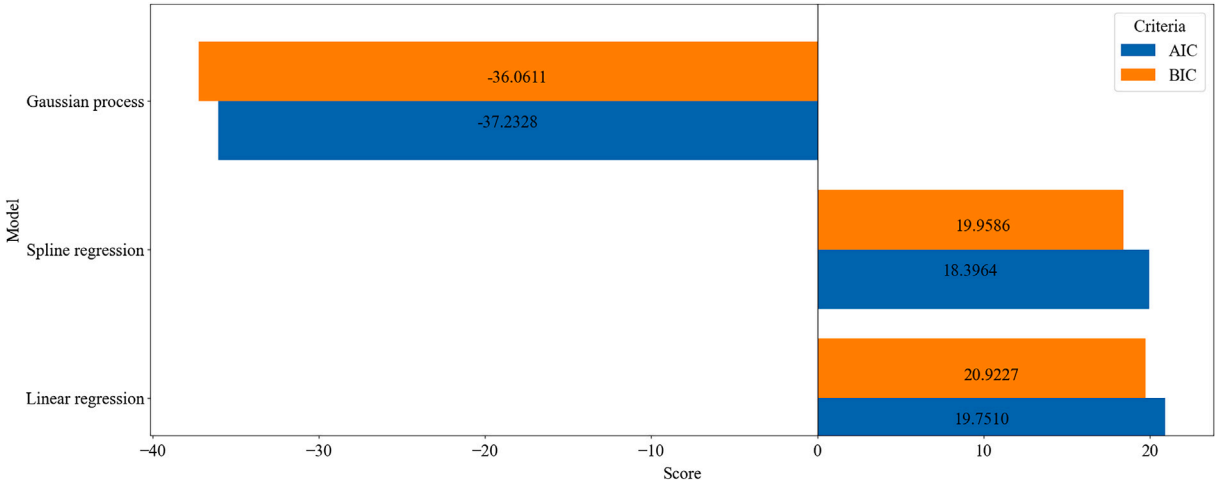

Fig. 12. A comparison of the model complexity between the proposed Gaussian Process-based deep learning (GPDL) and the linear and spline regression models.

A comparison of the MBE for the different models is presented in Table 7 (Bias detection). Table 7 (Bias detection) shows a minimum MBE of $-6e^{-4}$ $[kWh/m^2]$ with the proposed GPDL while it is $-3.4106e^{-14}$ $[kWh/m^2]$ and $-2.8421e^{-14}$ $[kWh/m^2]$ for the linear and spline regression models, respectively. This highlights that the proposed GPDL has an MBE that is about $6e^{-4}$ lower compared to these state-of-the-art models. The lower MBE indicates that the proposed GPDL model tends to underpredict the EUI by about $-6e^{-4}$ $[kWh/m^2]$ relative to the mean EUI, resulting in negligible systematic bias. We evaluated the model fitting and presented comparative results in Fig. 11. The values of the R-squared and adjusted R-squared scores for the proposed GPDL are 0.9999 and 0.9999, respectively. However, the model fitting results for the R-squared scores of the linear (0.9592) and spline (0.9774) models are comparatively lower compared to the proposed GPDL. This indicates the high competency of the GPDL in performing deep retrofitting analysis at a large-scale community level.

Given the importance of model complexity in resource consumption, a comparative study of model complexity for GPDL, linear, and spline models is presented in Fig. 12. The figure shows that the highest values of AIC and BIC result in a more complex model, regardless of successful prediction capacity. Conversely, the lowest values of AIC and BIC indicate a tendency towards a more parsimonious model. The results show that the linear model is the least suitable method for deep retrofitting, with AIC and BIC values of 20.9227 and 19.7510, respectively. The spline method exhibits a similar magnitude. However, the proposed GPDL demonstrates the best integration complexity, with comparatively smaller and negative values of AIC and BIC.

The residual assessment results are presented in Table 7 (Residual assessment) , which shows a lower Shapiro–Wilk Test value (W = 0.8641) compared to the linear regression (W = 0.80703) and Spline regression (W = 0.8834). The results trend suggests that the proposed GPDL handles the distribution better compared to the linear and spline regression models. The *p*-values results provide further insights into the normality of the proposed GPDL model compared to the linear and spline regression models.

In connection with the Shapiro–Wilk test for normality and p-values, the Q-Q plot in Fig. 13 is visualized. The figure highlights the data that is closer to the diagonal, indicating that the proposed GPDL supports both the Shapiro–Wilk test for normality and the p-values of the residuals. This suggests that there are no significant deviations in the residuals and that they follow a normal distribution, in comparison to the state-of-the-art linear and spline regression models. The comparative results of the model uncertainty and predictive distribution for the various models are presented in Table 7 (Uncertainty handling). The table shows that the PINAW of the proposed GPDL is 0.0008, which indicates that the GPDL has high credibility in predicting site EUI for deep retrofitting scenarios.

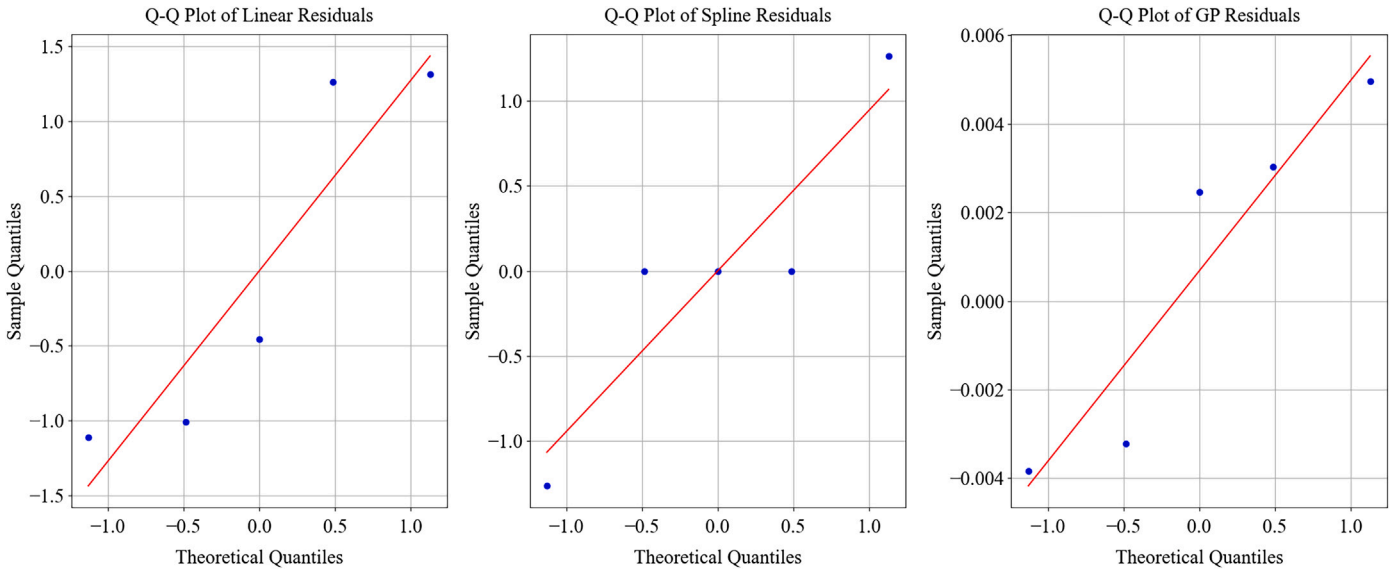

Fig. 13. A representation of the Quantile–Quantile (Q-Q) plot for various models.

The NLPD of the proposed GPDL is -4.1871, which makes the proposed GPDL a more preferred model as a conservative approach in developing the prediction model.

A comparison of the U-statistic is presented in Table 7 (Relative performance), which shows that the U-statistic value of the proposed GPDL is $1.16e^{-3}$, which is the lowest one compared to the linear regression ($3.4e^{-3}$) and the spline regression ($2.5e^{-3}$). This implies that the proposed GPDL has a lower value closer to zero, and therefore indicates high performance compared to the state-of-the-art linear and spline regression models to forecast the EUI for the application of the various retrofitting measures in the building community.

4.7. Implications and recommendations for energy policymakers and smart city planners

The end-user energy intensity in retrofitted buildings plays a critical role in determining the overall energy consumption profile and has the potential to support energy policymakers in identifying the most suitable PEF that leads to optimizing energy consumption while planning for smart city development. In this study, we highlighted the critical role of EUI and analyzed its impact on the determination of PEF through a case study conducted in Mullingar City, Ireland. The study aims to support energy decision-makers in strategically planning for energy-efficient retrofitting, thus promoting more sustainable and optimized energy management in smart city development. Given the cost of overhead energy generation, our study highlighted that electricity poses a high PEF due to thermal to electricity conversion losses.

In contrast, natural gas and renewable energy sources (RESs) have a lighter upstream loss due to the locality of their generation, resulting in lower PEF and therefore have a higher feasibility for HVAC. They have the ability not only to save energy but also to cut the dependency on fossil fuels, leading to a lower overall carbon footprint. Besides, the CAPEX of modern HVAC systems within existing buildings is cheaper due to lower construction and labor costs compared to enhancing the building envelope and walls.

Therefore, considering the case of Ireland, where most buildings are from before the 1980s and have cultural and historical significance, there are some conventions and measures in place to not completely modify the physical appearance of the constructions. Retrofitting the heating, cooling, and ventilation systems provides ample opportunity for policymakers to cut overheads and save energy. For instance, the study demonstrated about 39.2 % of energy savings for the overall Mullingar city, leading to reduced electricity costs for the state.

Nevertheless, given the atmospheric differences between Ireland and other EU countries, on the EU level, policymakers and smart city planners are required to identify the most suitable PEF with minimal energy overhead costs to save energy and reduce costs for smart city energy communities. This implies that for some EU countries such as Spain, Italy, Greece, Portugal, and France, there are abundant solar opportunities with the lowest PEF [96], while countries such as the Netherlands, Germany, Croatia, Denmark, Poland, and Romania have natural gas with a lower PEF [97].

On the other hand, Ireland, Finland, Sweden, and Belgium have abundant wind resources with a lower PEF [98]. Consequently, depending on the EUI and the PEF, energy policymakers and smart city planners have to identify and allocate an appropriate PEF to lower energy overhead generation costs, save energy, reduce carbon emissions, and promote a more sustainable society.

5. Conclusion

This study highlighted the importance of the end-use intensity and its implications for energy policymakers and smart city planners when allocating primary energy factors in the development of a sustainable smart city and cost savings for the energy community. Consequently, this study presented a detailed data-driven Gaussian-Process with Deep Learning approach based on the integration of Gaussian-Process with Deep Learning. As such, it aims to enhance the prediction of the end-use intensity, reduce computational complexity, and recommend the primary energy source for the heating, water system, heating ventilation and air conditioning, fans, interior lighting, electric equipment, pump, and gas equipment system. A detailed formulation for the end-use intensity and primary energy factors is established, and a mathematical model for integrating the Gaussian Process with Deep Learning is developed. Mullingar city is utilized as a case study, where 6076 buildings of various types (e.g., commercial, public and government, recreational and entertainment, transportation and infrastructure, religious, and residential) in the city are characterized by their thickness, conductivity, density, heat, roughness, thermal, solar, and visibility absorptance. A comprehensive evaluation criterion is established from the end-use intensity, primary energy factor, deep retrofitted analysis, and model performance perspectives, and the performance of the proposed Gaussian Process-based Deep

Learning is evaluated against state-of-the-art linear and spline regression models.

The simulation results demonstrated a higher performance compared to these state-of-the-art models. In more detail, the findings showcased a reduction of end-use intensity by about 52.4 %, resulting in 39.2 % energy savings for the overall city with high accuracy of mean square error (1.3005), root mean square error (0.0036), and mean absolute percentage error (0.0022), with a significant reduction in the simulation time, highlighting the importance of the proposed Gaussian Process-based Deep Learning for the city. The Mullingar city case study demonstrated a 39.2 % energy saving for retrofitting the overall city heating, cooling, and ventilation systems, showcasing a reduction in energy generation overhead costs. Consequently, this leads to reduced electricity consumption costs for the state. Based on the findings, the study suggested the use of natural gas and renewable energy sources for Ireland, while highlighting key factors for other EU countries.

In the future, further exploration, such as analyzing various cost factors (transmission and distribution), will provide more comprehensive recommendations for the utilization of the primary energy factor. This will help lower energy losses, cut costs, reduce the carbon footprint, and contribute to the development of a more sustainable society.

CRediT authorship contribution statement

Behnam Mohseni-Gharyehsafa: Writing – original draft, visualization, software, methodology, and data curation. **Shahid Hussain:** Writing – review & editing, visualization, validation, methodology, and investigation. **Amy Fahy:** Writing – review & editing, resources, project administration, investigation, and funding acquisition. **Mattia De Rosa:** Validation, supervision, project administration, methodology, and funding acquisition. **Fabiano Pallonetto:** Supervision, project administration, investigation, funding acquisition, and formal analysis.

Declaration of competing interest

The authors declare that they have no known competing financial interests or personal relationships that could have appeared to influence the work reported in this paper.

Acknowledgment

Gratitude is extended to Denis Buckley, Senior Technical Officer at the National University of Ireland Maynooth, for his tremendous assistance and steadfast support in providing the necessary hardware for the large-scale simulations. Special thanks to Nicolene Dawkins, IRESI group lab manager, for facilitating access to the storage hardware needs prior to the start of Behnam's Erasmus+ internship in Italy. This work has been funded by the Research Ireland, project NexSys SFI Grant No.: 21/SPP/3756 and RENEW Challenge SFI 22/NCF/EI/11334.

Data availability

Data will be made available on request.

References

[1] de Oliveira CC, Vaz ICM, Ghisi E. Retrofit strategies to improve energy efficiency in buildings: an integrative review. Energy Build 2024;114624.
[2] Kang E, Lee H, Yoon J, Cho H, Chaichana C, Kim D. Investigating the influence of uncertainty on office building energy simulation through occupant-centric control and thermal comfort integration. Energy Build 2024;322:114741.
[3] Hauashdh A, Nagapan S, Jailani J, Gamil Y. An integrated framework for sustainable and efficient building maintenance operations aligning with climate change, SDGs, and emerging technology. Results Eng 2024;21:101822.
[4] Duan Z, de Wilde P, Attia S, Zuo J. Prospect of energy conservation measures (ECMs) in buildings subject to climate change: a systematic review. Energy Build 2024;114739.
[5] Wang C, Yang H, Ji J. Investigation on overall energy performance of a novel multi-functional pv/t window. Appl Energy 2023;352:122000.
[6] Kabbara Z, Jorens S, Seuntjens O, Verhaert I. Simulation-based optimization method for retrofitting hvac ductwork design. Energy Build 2024;307:113991.
[7] Tozer L, Baggio G, Kantamneni A, MacRae H. Equity-based energy retrofits to address energy poverty in Canada. Energy Policy 2024;195:114341.
[8] Galvin R. How photovoltaics make energy refurbishment more affordable in apartment buildings. J Clim Finance 2024;7:100039.
[9] Bragolusi P, D'Alpaos C. The valuation of buildings energy retrofitting: a multiple-criteria approach to reconcile cost-benefit trade-offs and energy savings. Appl Energy 2022;310:118431.
[10] Li R, Huang C, Xin W, Ye J, Zhang X, Qu R, et al. Data-driven optimization reveals the impact of urban heat island effect on the retrofit potential of building envelopes. Build Environ 2024;112367.
[11] Djilali AB, Yahdou A, Bounadja E, Benbouhenni H, Zellouma D, Colak I. Energy management of the hybrid power system based on improved intelligent perturb and observe control using battery storage systems. Energy Rep 2024;11:1611–26.
[12] Elhamy AA, Mokhtar M. Phase change materials integrated into the building envelope to improve energy efficiency and thermal comfort. Future Cities Environ 2024;10.
[13] Alamayreh M, Altork Y. Evaluating the economic and environmental viability of hybrid solar-geothermal heat pump systems in Jordan using multi-criteria decision analysis. Discov Sustain 2024;5:377.
[14] Ferrari S, Zoghi M, Cardelli R, et al. A monitoring campaign introducing the indoor driving temperature to assess the building envelope performance. Appl Energy 2025;377:124650.
[15] Deb C, Dai Z, Schlueter A. A machine learning-based framework for cost-optimal building retrofit. Appl Energy 2021;294:116990.
[16] Dey M, Rana SP, Dudley S. Automated terminal unit performance analysis employing x-rbf neural network and associated energy optimisation–a case study based approach. Appl Energy 2021;298:117103.
[17] Hussain S, Teni AP, Hussain I, Hussain Z, Pallonetto F, Eichman J, et al. Enhancing electric vehicle charging efficiency at the aggregator level: a deep-weighted ensemble model for wholesale electricity price forecasting. Energy 2024;308:132823.
[18] Johari F, Lindberg O, Ramadhani UH, Shadram F, Munkhammar J, Widén J. Analysis of large-scale energy retrofit of residential buildings and their impact on the electricity grid using a validated ubem. Appl Energy 2024;361:122937.
[19] Davenport TH, Brynjolfsson E, McAfee A, Wilson HJ, et al. Artificial intelligence: the insights you need from Harvard business review. Harvard Business Press; 2019.
[20] Ahmad A, Bande L, Ahmed W, Young K, Jha M. Ai application in architecture in uae: application of an advanced optimized shading structure as a retrofit strategy of a midrise residential building façade in downtown abu dhabi. Energy Build 2024;114995.
[21] Leuthe D, Mirlach J, Wenninger S, Wiethe C. Leveraging explainable ai for informed building retrofit decisions: insights from a survey. Energy Build 2024;318:114426.
[22] Seyedzadeh S, Rahimian FP, Oliver S, Rodriguez S, Glesk I. Machine learning modelling for predicting non-domestic buildings energy performance: a model to support deep energy retrofit decision-making. Appl Energy 2020;279:115908.
[23] Rashid SA, Haider Z, Hossain SC, Memon K, Panhwar F, Mbogba MK, et al. Retrofitting low-cost heating ventilation and air-conditioning systems for energy management in buildings. Appl Energy 2019;236:648–61.
[24] Park J-S, Hussain S, Lee J-O, Kim BH, Kim Y-S. Time-of-use (tou) electricity rate for vehicle-to-grid (v2g) to minimize a charging station capacity. Int J Electr Power Energy Syst 2024;161:110209.
[25] Wenninger S, Karnebogen P, Lehmann S, Menzinger T, Reckstadt M. Evidence for residential building retrofitting practices using explainable ai and socio-demographic data. Energy Rep 2022;8:13514–28.
[26] Ghazwani K, Beach T, Rezgui Y. Energy retrofitting using advanced building envelope materials for sustainable housing: a review. Build Environ 2024;112243.
[27] Walter T, Sohn MD. A regression-based approach to estimating retrofit savings using the building performance database. Appl Energy 2016;179:996–1005.
[28] Roy SS, Roy R, Balas VE. Estimating heating load in buildings using multivariate adaptive regression splines, extreme learning machine, a hybrid model of mars and elm. Renew Sustain Energy Rev 2018;82:4256–68.
[29] Zhao X, Tan Y, Shen L, Zhang G, Wang J. Case-based reasoning approach for supporting building green retrofit decisions. Build Environ 2019;160:106210.
[30] Li Y, Du H, Kumaraswamy SB. Case-based reasoning approach for decision-making in building retrofit: a review. Build Environ 2023;111030.
[31] Liu T, Ma G, Wang D, Pan X. Intelligent green retrofitting of existing buildings based on case-based reasoning and random forest. Autom Construct 2024;162:105377.
[32] Choi S, Lim H, Lim J, Yoon S. Retrofit building energy performance evaluation using an energy signature-based symbolic hierarchical clustering method. Build Environ 2024;251:111206.
[33] Adly B, El-Khouly T. Combining retrofitting techniques, renewable energy resources and regulations for residential buildings to achieve energy efficiency in gated communities. Ain Shams Eng J 2022;13:101772.
[34] You K, Qian QK, Cai W, Wang X, Visscher H. Subsidy allocation for residential building energy retrofit: a perspective of families' incomes, sustainable cities and society. 2024;105317.
[35] Zhang H, Feng H, Hewage K, Arashpour M. Artificial neural network for predicting building energy performance: a surrogate energy retrofits decision support framework. Buildings 2022;12:829.
[36] Ali U, Bano S, Shamsi MH, Sood D, Hoare C, Zuo W, et al. Urban residential building stock synthetic datasets for building energy performance analysis. Data Brief 2024;53:110241.
[37] Thrampoulidis E, Mavromatidis G, Lucchi A, Orehounig K. A machine learning-based surrogate model to approximate optimal building retrofit solutions. Appl Energy 2021;281:116024.
[38] Al-Habaibeh A, Sen A, Chilton J. Evaluation tool for the thermal performance of retrofitted buildings using an integrated approach of deep learning artificial neural networks and infrared thermography. Energy Built Environ 2021;2:345–65.

[39] Sharma SK, Mohapatra S, Sharma RC, Alturjman S, Altrjman C, Mostarda L, et al. Retrofitting existing buildings to improve energy performance. Sustainability 2022;14:2071–1050.
[40] Ma D, Li X, Lin B, Zhu Y, Yue S. A dynamic intelligent building retrofit decision-making model in response to climate change. Energy Build 2023;284:112832.
[41] AlFaris F, Juaidi A, Manzano-Agugliaro F. Intelligent homes' technologies to optimize the energy performance for the net zero energy home. Energy Build 2017;153:262–74.
[42] Yuan H, Ma X, Ma M, Ma J. Hybrid framework combining grey system model with gaussian process and stl for CO2 emissions forecasting in developed countries. Appl Energy 2024;360:122824.
[43] Fortuin V. Priors in bayesian deep learning: a review. Int Stat Rev 2022;90:563–91.
[44] Moayedi H, Mosavi A. Synthesizing multi-layer perceptron network with ant lion biogeography-based dragonfly algorithm evolutionary strategy invasive weed and league champion optimization hybrid algorithms in predicting heating load in residential buildings. Sustainability 2021;13:3198.
[45] Culleton MD. Urban quality related effects on residential property prices in Dublin. ireland: 2022.
[46] Zuhaib S, Manton R, Hajdukiewicz M, Keane MM, Goggins J. Attitudes and approaches of Irish retrofit industry professionals towards achieving nearly zero-energy buildings. Int J Build Pathol Adapt 2017;35:16–40.
[47] Schildkamp M, Silvestri S, Araki Y. Rubble stone masonry buildings with cement mortar: design specifications in seismic and masonry codes worldwide. Front Built Environ 2020;6:590520.
[48] Loderer F. Evolution of ec 6—influence on masonry constructions made from aac, ce/papers. 2023;6:177–81.
[49] Broderick A. A pre and post evaluation of indoor air quality, ventilation, and thermal comfort in retrofitted co-operative social housing. Build Environ 2017;122:126–133.
[50] McGrath JA, Byrne MA. Unveil: understanding ventilation and radon in energy efficient buildings in Ireland, environmental Protection agency. Ireland: Wexford; 2019.
[51] Moreno DG, O'Toole D, McGetrick PJ, Harte AM. Timber construction in Ireland for the mitigation of climate change and the housing crisis in 2022. Assessment (LCA 2022;2:3.
[52] Daly P, Ronchetti P, Woolley T. Hemp lime bio-composite as a building material Irish construction. Ireland: Environmental Protection Agency; 2012.
[53] Muddu RD, Gowda D, Robinson AJ, Byrne A. Optimisation of retrofit wall insulation: an Irish case study. Energy Build 2021;235:110720.
[54] Walker R, Pavía S. Thermal and moisture monitoring of an internally insulated historic brick wall. Build Environ 2018;133:178–86.
[55] Walker R, Pavía S. Thermal performance of a selection of insulation materials suitable for historic buildings. Build Environ 2015;94:155–65.
[56] Bennett G, Elwell C, Oreszczyn T. Space heating operation of combination boilers in the Uk: the case for addressing real-world boiler performance. Build Serv Eng Res Technol 2019;40:75–92.
[57] Travis L, Ray K. Pointwise uncertainty quantification for sparse variational gaussian process regression with a brownian motion prior. Adv Neural Inf Process Syst 2024;36.
[58] Li W, Fan Y, Ringbeck F, Jöst D, Sauer DU. Unlocking electrochemical model-based online power prediction for lithium-ion batteries via gaussian process regression. Appl Energy 2022;306:118114.
[59] Shi X, Jiang D, Qian W, Liang Y. Application of the gaussian process regression method based on a combined kernel function in engine performance prediction. ACS Omega 2022;7:41732–43.
[60] Daemi A, Kodamana H, Huang B. Gaussian process modelling with gaussian mixture likelihood. J Process Control 2019;81:209–20.
[61] Kent D. Regenerating essential goods and services in urban landscapes: sustainability through ecological design. Taylor & Francis; 2024.
[62] Hmouda AM, Orzes G, Sauer PC. Sustainable supply chain management in energy production: a literature review. Renew Sustain Energy Rev 2024;191:114085.
[63] Jin M, Feng W, Marnay C, Spanos C. Microgrid to enable optimal distributed energy retail and end-user demand response. Appl Energy 2018;210:1321–35.
[64] Feijoo F, Kundu A, Flores F, Matamala Y. Photovoltaic sizing assessment for microgrid communities under load shifting constraints and endogenous electricity prices: a stackelberg approach. Energy 2024;307:132758.
[65] Sustainable Energy Authority of Ireland (SEAI). Domestic Energy Assessment Procedure (DEAP), Version 4.2.6 2024; https://www.seai.ie/sites/default/files/publications/DEAP_Manual.pdf, Ireland's official method for calculating and rating the energy performance of dwellings.
[66] Westmeath Examiner. Mullingar's population growing faster than athlone's; 2025. https://www.westmeathexaminer.ie/2023/06/29/mullingars-population-growing-faster-than-athlones/, Accessed: March 6.
[67] Chicco D, Warrens MJ, Jurman G. The coefficient of determination r-squared is more informative than smape, mae, mape, mse and rmse in regression analysis evaluation. Peerj Computer Science 2021;7:e623.
[68] Lee T-S, Lu W-C. An evaluation of empirically-based models for predicting energy performance of vapor-compression water chillers. Appl Energy 2010;87:3486–93.
[69] Wahid MF, Tafreshi R, Khan Z, Retnanto A. Prediction of pressure gradient for oil-water flow: a comprehensive analysis on the performance of machine learning algorithms. Journal Of Petroleum Science And Engineering 2022;208:109265.
[70] Teke A, Yıldırım HB, Çelik Ö. Evaluation and performance comparison of different models for the estimation of solar radiation. Renew Sustain Energy Rev 2015;50:1097–107.
[71] Maabreh M, Almasabha G. Machine learning regression algorithms for shear strength prediction of sfrc-dbs: performance evaluation and comparisons. Arabian J For Sciamp; Eng 2024;49:4711–27.
[72] Ritter A, Muñoz-Carpena R. Performance evaluation of hydrological models: statistical significance for reducing subjectivity in goodness-of-fit assessments. J Hydrol 2013;480:33–45.
[73] Roy SS, Samui P, Nagtode I, Jain H, Shivaramakrishnan V, Mohammadi-Ivatloo B. Forecasting heating and cooling loads of buildings: a comparative performance analysis. J Ambient Intel And Humanized Comput 2020;11:1253–64.
[74] Kaplan YA. Forecasting of global solar radiation: a statistical approach using simulated annealing algorithm. Eng Appl Artif Intel 2024;136:109034.
[75] Anggraeni W, Yuniarno EM, Rachmadi RF, Sumpeno S, Pujiadi P, Sugiyanto S, et al. A hybrid emd-grnn-pso in intermittent time-series data for dengue fever forecasting. Expert Syst With Appl 2024;237:121438.
[76] Mecibah MS, Boukelia TE, Tahtah R, Gairaa K. Introducing the best model for estimation the monthly mean daily global solar radiation on a horizontal surface (case study: Algeria. Renew Sustain Energy Rev 2014;36:194–202.
[77] Demir S, Sahin EK. The effectiveness of data pre-processing methods on the performance of machine learning techniques using rf, svr, cubist and sgb: a study on undrained shear strength prediction. Stochastic Environ Res Risk Assess 2024;1–18.
[78] Roy A, Al Zubayer T, Tabassum N, Islam MN, Sattar MA. Curfi: an automated tool to find the best regression analysis model using curve fitting. Eng Rep 2022;4:e12522.
[79] Acharya MS, Armaan A, Antony AS. A comparison of regression models for prediction of graduate admissions. In: 2019 international conference on computational intelligence in data science (ICCIDS); IEEE; 2019. p. 1–5.
[80] Rose S, McGuire TG. Limitations of p-values and r-squared for stepwise regression building: a fairness demonstration in health policy risk adjustment. The American Statistician 2019;73:152–56.
[81] Valbuena R, Hernando A, Manzanera JA, Görgens EB, Almeida DR, Silva CA, et al. Evaluating observed versus predicted forest biomass: R-squared, index of agreement or maximal information coefficient? Eur J Remote Sens 2019;52:345–58.
[82] Harbecke J, Grunau J, Samanek P. Are the bayesian information criterion (bic) and the akaike information criterion (aic) applicable in determining the optimal fit and simplicity of mechanistic models? Int Stud Philos Sci 2024;1–20.
[83] Cavanaugh JE, Neath AA. The akaike information criterion: background, derivation, properties, application, interpretation, and refinements. Wiley Interdisciplinary Reviews: Computational Statistics 2019;11:e1460.
[84] Drton M, Plummer M. A bayesian information criterion for singular models. Journal Of The Royal Statistical Society Series B: Statistical Methodology 2017;79:323–80.
[85] Ozbayram O, Olivier A, Graham-Brady L. Heteroscedastic gaussian process regression for material structure–property relationship modeling. Comput Methods Appl Mech Eng 2024;431:117326.
[86] Roy S, Uddin MG, Abdelrahman K, Fnais MS, Abioui M. Assessing the impact of digital elevation model resolution on hypsometric analysis in large river basins (India): a non-parametric statistical approach. Earth Sci Inf 2025;18:1–21.
[87] Hoxhaj V, Khattree R. Beyond q—q plots: some new graphical tools for the assessment of distributional assumptions and the tail behavior of the data. J Stat Theory Pract 2017;11:531–52.
[88] Chang X, Guo J, Qin H, Huang J, Wang X, Ren P. Single-objective and multi-objective flood interval forecasting considering interval fitting coefficients. Water Resour Manage 2024;1–20.
[89] Licata RJ, Mehta PM. Uncertainty quantification techniques for data-driven space weather modeling: thermospheric density application. Sci Rep 2022;12:7256.
[90] Bliemel F. Theil's forecast accuracy coefficient: a clarification. 1973.
[91] U.S. Energy Information Adminstration Independent statistics and analysis. 2025. https://www.eia.gov/, Accessed: March 6.
[92] Sustainable Energy Authority of Ireland, Derivation of primary energy and co2 factors for electricity in deap and neap. 2025. https://www.seai.ie/publications/PrimaryEnergyCO2FactorsElectricity.pdf, Accessed: March 6.
[93] Domestic Energy Assessment Procedure (DEAP)-Sustainable Energy Authority of Ireland, Domestic energy assessment procedure (deap). 2025. https://www.seai.ie/publications/DEAP_Manual.pdf, Accessed: March 6.
[94] Marrel A, Iooss B. Probabilistic surrogate modeling by gaussian process: a review on recent insights in estimation and validation. Reliability Engineering & System Safety 2024;110094.
[95] Ma J, Cheng JC. Estimation of the building energy use intensity in the urban scale by integrating gis and big data technology. Appl Energy 2016;183:182–92.
[96] Dincer F. The analysis on photovoltaic electricity generation status, potential and policies of the leading countries in solar energy. Renew Sustain Energy Rev 2011;15:713–20.
[97] Liuhto K. Natural gas in the eu in the twenty-first century: a special emphasis on lng. The Future Of Energy Consumption, Security And Natural Gas: LNG In The Baltic Sea Region 2022;21–60.
[98] Bórawski P, Bełdycka-Bórawska A, Jankowski KJ, Dubis B, Dunn JW. Development of wind energy market in the European union. Renewable Energy 2020;161:691–700.